AD 256 964

AEDC-TN-61-43

83 100

STATIC STABILITY CHARACTERISTICS OF THE PROPOSED B-58 AIRCRAFT ESCAPE CAPSULE AT TRANSONIC MACH NUMBERS

By

L. E. Rittenhouse, D. J. Pierce, and W. E. Summers
PWT, ARO, Inc.

May 1961

ARNOLD ENGINEERING DEVELOPMENT CENTER
AIR FORCE SYSTEMS COMMAND

USAF

$7.60

STATIC STABILITY CHARACTERISTICS OF THE PROPOSED B-58 AIRCRAFT ESCAPE CAPSULE AT TRANSONIC MACH NUMBERS

By

L. E. Rittenhouse, D. J. Pierce, and W. E. Summers

PWT, ARO, Inc.

May 1961

Program Area No. 102A

ARO Project Nos. 221138 and 221089

Contract No. AF 40(600)-800 S/A 11(60-110)

ABSTRACT

Results are presented from a wind tunnel investigation to ascertain the lateral and longitudinal stability and axial-force characteristics of the crew and pilot escape capsules proposed for the B-58 aircraft. The effect of varying several parachute parameters on parachute drag and capsule aerodynamics is also presented. Furthermore, a comparison of the capsule aerodynamic coefficients obtained with cold air simulation of the rocket exhausts in contrast to rocket motor firings is discussed. The tests were conducted at Mach numbers 0.60, 0.93, and 1.50 at Reynolds numbers ranging from 0.40 to 2.20 million. The test article attitude was varied from -10 to 90 deg in the pitch plane and from -5 to 25 deg in the yaw plane.

In general, both capsule configurations were statically unstable in the pitch and yaw planes. Furthermore, when the rocket jet was simulated, the parachute which was attached to the capsule dipped violently in and out of the jet wake.

CONTENTS

TABLE

ILLUSTRATIONS

NOMENCLATURE

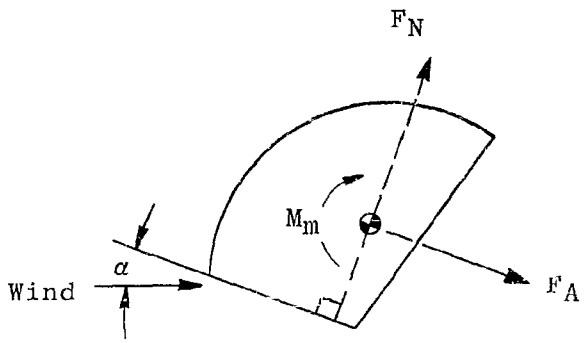

Longitudinal Forces
(Side View)

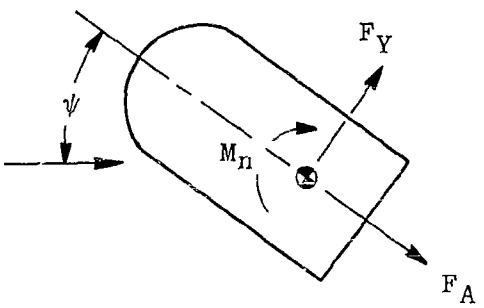

Lateral Forces
(Top View)

C_A	Measured axial-force coefficient, $\frac{F_A}{q_\infty S}$
$C_{D,p}$	Parachute drag coefficient, $\frac{F_p}{q_\infty S_p}$
C_m	Pitching-moment coefficient, $\frac{M_m}{q_\infty Sd}$ (Moment reference shown in Fig. 4a)
C_N	Normal-force coefficient, $\frac{F_N}{q_\infty S}$
C_n	Yawing-moment coefficient, $\frac{M_n}{q_\infty Sd}$ (Moment reference shown in Fig. 4a)
C_Y	Side-force coefficient, $\frac{F_Y}{q_\infty S}$
d	Model reference length, 1.333 ft model scale
F_A	Axial force, lb
F_N	Normal force, lb
F_p	Total parachute drag force, lb (addition of two drag link measurements, see Fig. 6)

F_Y	Side force, lb
$M_{\ell, R}$	Local Mach number in the plane of the pressure rake
M_m	Pitching moment, ft-lb
M_n	Yawing moment, ft-lb
M_∞	Free-stream Mach number
p_∞	Free-stream static pressure, psf
$p_{t, j}$	Total pressure of the jet measured in the model plenum chamber, psf
q_∞	Free-stream dynamic pressure, $0.7\, p_\infty M_\infty^2$, psf
Re	Reynolds number, $\frac{V_\infty d}{\nu_\infty}$
S	Model reference area, 0.796 ft^2 model scale
S_p	Parachute reference area based on the planform area of one gore lying flat times the number of gores in the canopy (see Table 1), ft^2
V_∞	Free-stream velocity, ft/sec
Y	Vertical distance measured from the centerline of the pressure rake, in.
α	Model angle of attack, deg
θ_F	Stabilization frame angle with respect to a vertical plane perpendicular to the lower surface of the capsule (86 deg is fully deployed and -15 deg and -20 deg are fully folded for the crew and pilot capsules, respectively), deg
λ	Ratio of the jet total pressure to the free-stream static pressure, $\frac{p_{t, j}}{p_\infty}$
ν_∞	Free-stream kinematic viscosity, ft^2/sec
ψ	Model angle of yaw, deg

MODEL DESIGNATIONS

B	Crew capsule including flotation booms, shear plates, canopy remover, rocket tubes, recovery parachute box, stabilization frame fully deployed*, and drag plate (see Fig. 4)
B'	Pilot capsule including those accessories mentioned for the crew capsule (see Fig. 4)
p_n	Parachute designation (see Table 1 and Figs. 6 and 7)

*Unless specifically noted the stabilization frame was fully deployed (θ_F = 86).

INTRODUCTION

The advent of high-speed aircraft has resulted in a reconsideration of the problem of escape from these vehicles in case of emergency. Several approaches to the problem have been undertaken and include (1) ejection seats, (2) separating sections of the aircraft, and (3) complete enclosures that eject from the aircraft. The last system has been proposed for the B-58 aircraft and includes a rocket-propelled capsule equipped with parachutes (drogue and recovery) and survival devices. The general sequence of events during separation from the aircraft involves closing the capsule, ejecting the capsule from the aircraft utilizing a solid propellant rocket installed in the capsule, and deploying, almost simultaneously, a drogue parachute (for static stability purposes) and stabilization frame. At the proper time (a function of altitude) in the trajectory, the drogue parachute is released and a large recovery parachute is deployed. During deployment of the recovery parachute, the stabilization frame is retracted and thus places the landing shock absorbers in proper orientation for impact. The capsule impacts with the occupant's back to the ground. Several mechanical and propulsion systems (mortar for initial boost-off before rocket firing and mortar for drogue parachute deployment) are required for successful ejection of the capsule. Furthermore, the aerodynamic characteristics of the capsule must be compatible with the aircraft over wide Mach number and altitude ranges at numerous pitch and yaw attitudes of the aircraft.

Initial wind tunnel tests of the proposed capsule at the Cornell Aeronautical Laboratory indicated that the stability characteristics (without rocket simulation) were adequate for the planned trajectories from the aircraft. However, subsequent full-scale tests at the Supersonic Military Air Research Track (SMART), Hurricane Mesa, Utah, revealed pitch-up and yaw instability problems during rocket motor operation that were serious enough to impose detrimental forces on the occupant. Consequently, an investigation of a 1/3-scale version of the capsule was initiated in the 16-Ft Transonic Circuit at the Arnold Center. The tests were sponsored by the Aeronautical Systems Division, Air Force Systems Command, and were completed during several occupancy periods from July 25, 1960 through February 9, 1961.

The principal objectives of the tests at Arnold Center were to determine the longitudinal and lateral stability characteristics of the pilot and crew capsules with and without rocket simulation and to determine an optimum drogue parachute configuration with regard to the capsule aerodynamics and parachute performance.

Manuscript released by authors April 1961.

During the tests longitudinal and lateral instability problems were encountered with the rocket simulation, and an effort was made to incorporate external surfaces on the capsule to improve the stability characteristics (Fig. 1). However the capsule design and contractual commitments had advanced to the point where the changes, although helpful in some instances, could not be used on the capsule. Therefore, the results presented herein are for the crew and pilot capsules without modifications.

APPARATUS

TEST FACILITY

The operational capabilities of the 16-Ft Transonic Circuit are described in Ref. 1. The wind tunnel is capable of variable-density operation throughout the Mach number range from 0.5 through 1.6. The location of the test article and model support equipment is shown in Fig. 2. The mechanism for pitching the model was hydraulically operated and mounted on the model support, whereas the yawing mechanism was electrically driven and mounted above the test section. The type and arrangement of the model support equipment was selected to provide large variations in model attitude. A photograph of the general test installation is shown in Fig. 3.

The air for the rocket motor simulation was ducted from an external supply through the model support into a plenum chamber inside the model. A maximum pressure of approximately 900 psia was obtained in the model at the highest flow rate (17 to 19 lb/sec).

TEST ARTICLE

The pilot and crew capsules were 1/3-scale versions of the full-scale capsules. Major model details and dimensions are presented in Fig. 4. Installation photographs are presented in Fig. 5. The pilot capsule differs from the crew capsule in the angle at which the backplate is inclined with the vertical and in the orientation of the rocket nozzles (see Fig. 4b). Differences in geometry between the two capsules are necessary because the pilot capsule does not leave the aircraft in the vertical plane of symmetry of the aircraft as does the crew capsule. Both configurations utilized the same model shell with the appropriate changes as just discussed.

The model shell was made of phenolic resin reinforced with glass cloth. The shell contained a steel structure for mounting the model on a strain-gage balance. The rocket simulation system (plenum, nozzles, air

ducting, etc.) was attached directly to the model support strut and not to the balance. In this manner, the induced aerodynamic effects of the air jet on the capsule aerodynamics were measured without measuring the jet thrust.

To substantiate the validity of the air simulation of the rocket exhaust, several solid propellant rocket motors were fired at various model attitudes. The specifications of the 1/3-scale rocket motors are given below:

Gas Generator Model Designation	-	2.2-NS (Convair)
Propellant Designation	-	RDS 135
Igniter Type	-	Electrical-Pyrotechnic
Gas Generator Weight Before Firing	-	14.0 lb
Gas Generator Weight After Firing	-	10.7 lb
Average Chamber Pressure	-	~520 psia
Average Weight Flow Rate	-	~1.4 lb/sec
Burning Time	-	~2.2 sec
Characteristic Exhaust Velocity	-	~4080 ft/sec

The nozzle geometry for the rocket motors was scaled from the full-scale capsule motors. The installation procedure for the rocket motors was comparable to that for the air simulation equipment.

The drogue parachute assembly is shown in Fig. 6. Three basic types of ribbon canopies were investigated: equiflow, conical, and hemisflow (see Fig. 7). Several modifications were made to specific parachutes and included changes in area, porosity, shroud-line length, and trailback distance. A complete tabulation of the parachute configurations is presented in Table 1.

A multiple-probe pressure rake was used to investigate the model wake in the region of the parachute. The pressure rake consisted of 12 total head and three static probes as shown in Figs. 8 and 9.

INSTRUMENTATION

The forces on the model were measured with a strain-gage balance. Balance outputs were translated through analog-to digital converters to an electronic computer for final data reduction while the test was in progress. No attempt was made to measure the jet thrust since, as previously mentioned, neither the jet simulation system nor the rocket motors were attached to the balance. During the rocket motor firings, the model forces (balance outputs) were recorded on an oscillograph, and the aerodynamic

forces were determined from the traces. This procedure was necessary because of the short burning time of the rockets.

The parachute drag was determined from two strain-gage links (see Fig. 6). The outputs from the parachute drag links were handled in the same manner as the balance outputs.

PROCEDURE AND PRECISION OF MEASUREMENTS

STATIC STABILITY

The tests were conducted at Mach numbers 0.60, 0.93, and approximately 1.50. However, the Mach number of primary concern was 0.93 which is the aircraft cruise Mach number. The data were obtained at Reynolds numbers between 0.40 and 2.20 million. The maximum changes in model attitude were from -10 to 90 deg in the pitch plane and from -5 to 25 deg in the yaw plane. In some instances, the maximum range was not obtainable because of overloading the strain-gage balance in the model. Force polars were obtained with and without jet simulation at various angles for the stabilization frame, θ_F. Parachute deployment was obtained by permitting the parachute to hang freely from the stabilization frame and to deploy as tunnel conditions were achieved (see Fig. 3).

The following uncertainties in the reduced data were determined by the statistical method outlined in Ref. 2:

M_∞	$Rex10^{-6}$	ΔC_N	ΔC_m	ΔC_A	ΔC_Y	ΔC_n	$\Delta\alpha$	$\Delta\psi$	ΔM_∞	$\Delta C_{D,p}$
0.60	0.40	±0.052	±0.012	±0.084	±0.052	±0.012	±0.1	±0.1	±0.003	±0.030
0.60	0.57	±0.018	±0.008	±0.038	±0.018	±0.008	±0.1	±0.1	±0.003	±0.023
0.93	0.70	±0.029	±0.006	±0.054	±0.029	±0.006	±0.1	±0.1	±0.004	±0.014
0.93	1.60	±0.016	±0.005	±0.020	±0.016	±0.005	±0.1	±0.1	±0.004	±0.009
1.50	1.51	±0.032	±0.004	±0.041	±0.032	±0.004	±0.1	±0.1	±0.005	
1.50	1.06	±0.049	±0.005	±0.058	±0.049	±0.005	±0.1	±0.1	±0.005	
1.50	2.20	±0.024	±0.002	±0.028	±0.024	±0.002	±0.1	±0.1	±0.005	

The uncertainties quoted for the force coefficients include the uncertainties in tunnel conditions and balance measurements. The uncertainty in Mach number refers to setting and calculating the average free-stream Mach number. However, during the rocket simulation phase of testing, the tunnel pressure level was very low (p_∞ ~ 100 psfa), and the effect of the air issuing from the nozzles caused the free-stream Mach number to vary as

much as -0.04 during a force polar. The longitudinal variation of the free-stream Mach number in the vicinity of the test article was approximately ±0.006 as determined from tunnel-empty calibrations.

COLD AIR SIMULATION AND ROCKET FIRINGS

The simulation in the wind tunnel of the proper flow field generated by the full-scale rocket motor was of primary concern since the effect of the pressure field or the physical impingement of the exhaust on the lower aft portion of the capsule could possibly explain the instability of the capsule which occurred during full-scale tests. However, to scale accurately the full-scale rocket and to obtain static stability data during the burning time of the rocket (0.3 sec) would have been extremely difficult. Furthermore, the number of rockets required to obtain the minimum amount of data would have been impractical. Therefore, a continuous supply of high-pressure air was ducted to the model for rocket simulation. The nozzle design and jet pressure required to simulate various altitudes was determined by the contractor (Convair Division of General Dynamics, Fort Worth, Texas). It should be mentioned that the full-scale rocket motor operates at a constant chamber pressure (2600 psia); therefore, the ratio of chamber pressure, $p_{t,j}$, to free-stream static pressure, p_∞, varies with altitude. During the tests, the high-pressure air was allowed to flow continuously as the model attitude was varied at a given Mach number and altitude.

Several small rocket motors were installed in the capsule and fired at various Mach numbers and model attitudes during the investigation to determine the validity of the air simulation technique. These rocket motors were designed and furnished by Convair (see section titled Test Articles). The uncertainties in determining the model forces from the oscillograph readings obtained during the rocket firings are noted on the figures. The uncertainties are based primarily on the ability to read the oscillograph trace to within ±0.05 inch.

RESULTS AND DISCUSSION

The results from the investigation are presented in three general categories: (1) the effect of various parachute parameters on the parachute drag and capsule aerodynamics, (2) the capsule aerodynamic characteristics with and without jet simulation and a parachute at several stabilization frame angles, and (3) a comparison between the cold air

simulation and the rocket firings. The majority of the parachute data was obtained at Mach number 0.93 and used for the selection of an optimum parachute.*

A considerable amount of data were obtained with jet-air simulation and without a parachute for several stabilization frame angles. Although the capsule is in this configuration for only a very short time, the stability of the capsule is of importance before or during parachute and frame deployment since the capsule could attain considerable angular momentum. The angular momentum attained in the pitch or yaw plane could produce excessive forces on the occupant during the rocket firing or after the rocket burns out and the capsule returns to a trimmed position. It should be remembered that for successful ejection the capsule aerodynamics must be compatible with the aircraft at various yaw and pitch attitudes of the aircraft.

The degree of longitudinal or lateral stability required for the capsule to deploy successfully from the aircraft is beyond the scope of this report. This involves a detailed trajectory analysis at various Mach numbers and altitudes during numerous yaw and pitch maneuvers of the aircraft. That analysis is being conducted by the capsule contractor. The final result will be an operational envelope for the aircraft within which the capsules may be successfully employed.

THE INFLUENCE OF SEVERAL PARACHUTE PARAMETERS ON PARACHUTE DRAG AND CAPSULE AERODYNAMICS

Canopy Configuration

Three different types of parachute canopies were tested at Mach number 0.93, and the data are presented in Fig. 10a. The shroud line length, trailback distance, parachute area and porosity were nearly constant. The data for the crew capsule (B) without a parachute are presented for comparative purposes. Although all three canopies produced a significant increase in capsule axial-force coefficient, the conical parachute (BP_{23}) exhibited the largest increment. (A large axial-force coefficient for the capsule is an undesirable characteristic since it aggravates the aircraft tail clearance problems.) The parachutes increased the normal-force coefficients (Fig. 10a) for the capsule at the higher angles of attack. This was expected since the drag force of the parachute exerts a force normal to the capsule at positive angles of attack.

*Data obtained at Mach number 2.0 from another wind tunnel facility were also used in the determination of the optimum parachute.

It was observed during the tests that the parachutes trailed up* behind the capsule when the model was near zero angle of attack. The data indicate (Fig.10a) that the capsule alone had a negative normal-force coefficient near zero angle of attack. Thus, an upwash occurred behind the body. The trailing up of the parachute is directly associated with the wake from the capsule. The erratic changes in pitching-moment coefficient for the BP_{12} configuration (Fig.10a) near zero angle of attack were a result of a significant change in the parachute trail angle when the capsule was pitched about zero angle of attack.

In summary, the capsule without a parachute had two stable trim points: one occurred somewhere between -10 deg and -20 deg (extrapolation of the data) and a second at approximately 50-deg angle of attack. The addition of any one of the three parachutes resulted in a change in capsule trim characteristics because only one trim point occurred and that was near zero angle of attack.

Parachute Area

The effects of changes in the parachute area for the 15-percent equiflow canopy are presented in Fig. 10b. As was expected, an increase in the parachute area resulted in an increase in the capsule axial-force coefficients. However, only slight changes in the parachute drag coefficients were obtained and indicated that the parachute drag force increased proportionately to the area of the parachute. Slight increases in the normal-force coefficients occurred as the parachute area was increased (Fig. 10b). Moreover, the magnitude of the pitching-moment coefficient increased at the higher angles of attack as the parachute area was increased. Again, as was the case in the preceding section, the pitching-moment coefficients varied considerably near zero angle of attack in a somewhat irregular manner, and this was attributed to the trail angle of the parachute. This is substantiated by the fact that the axial-force and normal-force coefficients changed in a regular fashion from 10 to 20-deg angle of attack. Thus, the trail angle of the parachute varied in an erratic manner and produced the pitching-moment coefficients presented in Fig. 10b.

Parachute Porosity

The effects of changes in porosity on the capsule aerodynamics and parachute drag coefficients for Mach number 0.93 are presented in Fig. 10c

---

*The parachute trail angle is defined as the angle between the parachute bridle and the wind tunnel centerline.

Some increase in parachute drag coefficient with a decrease in porosity (less open area) is noted in Fig.10c. The significant effect of porosity appeared in the pitching-moment coefficients near zero angle of attack. Here, as the porosity was increased the configuration became more stable through a trim point between 0 and 10-deg angle of attack.

Shroud Line Length

Data indicating the effect of changing the shroud line length on the 15-percent equiflow parachute while keeping the trailback distance constant are presented in Fig. 10d for Mach number 0.93. In general, the effect of a two-fold increase in shroud line length produced only minor changes in the parachute drag coefficients and capsule characteristics.

Trailback Distance

The effect of changes in trailback distance with the 15-percent equiflow parachute are presented in Fig.10e. An increase in trailback distance produced slight increases in $C_{D,p}$, C_N, and C_A and generally resulted in an increase in the magnitude of C_m. The shortest trailback distance (BP_{15}) resulted in a stable trim point at -10-deg angle of attack and a region of neutral stability near 30 deg. The intermediate trailback distance (BP_{11}) indicated no tendency to trim through the angle-of-attack range of the test (a slightly more negative angle of attack might have resulted in a stable trim point), whereas with the longest trailback distance (BP_{16}) the configuration trimmed near -5-deg angle of attack.

The data presented in Fig. 10 were used by the contractor to select the optimum configuration. The hemisflow parachute P_{31} was chosen as the optimum on the basis of parachute performance and compatability with the capsule at Mach number 0.93 as well as at Mach number 2.0 (results obtained from another facility). Data on capsule stability presented hereinafter were obtained with the P_{31} parachute.

AERODYNAMIC CHARACTERISTICS OF THE CAPSULE

The initial portion of the trajectory of the capsule from the aircraft involves the deployment of the stabilization frame and parachute. Consequently, these data are presented first for various jet pressure ratios, λ. Following the results obtained at various stabilization frame angles, data are presented with the parachute attached to the capsule at several jet pressure ratios (unless specifically noted the stabilization frame angle, θ_F, is 86 deg.) In some cases, only the lateral or the longitudinal stability characteristics of the capsule were obtained. However, for those cases in which both types of data were obtained, both are presented.

The lateral stability characteristics of the crew capsule (B) with the stabilization frame in several positions from completely folded, θ_F = -15, to fully deployed, θ_F = 86, are presented in Fig. 11 for Mach number 0.60. The data points at zero jet pressure ratio (Fig. 11a) are shown for comparative purposes only, since the rocket would be burning before the capsule leaves the aircraft and during the frame deployment. It is apparent from Fig. 11a that the crew capsule was highly unstable in the yaw plane for the various values of jet pressure ratio. However, with the stabilization frame fully deployed, a stable trim point was noted at about 25 deg in yaw.

A large increase in axial-force coefficient was experienced by the capsule as the jet pressure ratio was increased. This was caused (1) by the jet air which reduced the static pressure on the aft portion of the capsule and thus produced a large differential in pressure between the forward and aft portions of the capsule and (2) by the high-energy jet which impinged on the cross member and fins of the stabilization frame. This can be seen by examining the data presented in Fig. 11a for θ_F = -15 and 20. With the stabilization frame fully folded, θ_F = -15, a two-fold increase in C_A caused by a reduction in static pressure only is noted in Fig. 11a. In addition, with the jet impinging on the frame (θ_F = 20), a six-fold increase in C_A was evident when comparing the data obtained at zero jet pressure ratio and maximum jet pressure at zero yaw angle.

The longitudinal stability characteristics of the crew capsule with the stabilization frame fully deployed are also presented in Fig. 11a. It would be difficult to determine what attitude the capsule would assume with the jet on since a stable trim point was not obtained. However, the results indicate that the capsule will move toward a high angle of attack. The degree of pitch-up will be a function of the initial attitude of the capsule with respect to the wind vector (initial forces) and the time of rocket burning which will affect the angular momentum of the capsule.

Longitudinal stability results with the crew capsule and parachute (BP_{31}) are presented in Fig. 11b for Mach number 0.60. The data obtained at λ = 0 are applicable to that portion of the trajectory after rocket burnout. A very large increase in the pitching-moment coefficient as the jet pressure ratio was increased is evident in Fig. 11b. A comparison of Figs. 11a and b (θ_F = 86) shows that the incremental increases in C_A for changes in λ were approximately equal; this indicates that the parachute drag did not appreciably increase with λ. However, the pitching-moment coefficient was changed significantly; this indicated that the trail angle of the parachute changed and produced large positive moments on the capsule when the jet air was used. The parachute was pulled down toward the jet, and consequently the distance between the line of action

for the parachute drag and the capsule moment reference was increased. In most instances, the action of the parachute in the presence of the jet air was erratic and violent because the parachute dipped in and out of the jet wake. Only a limited amount of data was obtained with the parachute and jet simulation because either the balance moment limits were exceeded or the parachute assembly failed.

The erratic action of the parachute and large traildown angles encountered during the jet simulation prompted an investigation of the flow field in the region in which the parachute was located. To gain an insight into the phenomenon a vertical rake with static and total pressure probes was installed in the region aft of the model where the parachute was located to determine the nature of the pressure field which emanated from the jet. Some typical results are presented in Fig. 12a. The trail angles were determined from motion picture coverage. Although a trail angle of -8 deg is presented for the capsule at zero angle of attack and $\lambda = 548$, the parachute dipped down into the jet wake with the trail angle intermittently approaching -20 to -30 deg. In the region in which the jet influenced the flow field, the static pressure was much lower than the static pressure in the capsule wake; thus the parachute moved down into the low pressure field. A sequence of photographs obtained from motion pictures is presented in Fig. 12b to illustrate the downward movement of the parachute.

Results obtained with the crew capsule (B) and crew capsule with the parachute (BP_{31}) at Mach number 0.93 are presented in Fig. 13 for various stabilization frame angles and jet pressure ratios. In general, the trends (Fig. 13a) were the same as discussed for Mach number 0.60, although the effect of λ was somewhat less. The magnitude of the forces created by the jet was somewhat less for Mach number 0.93 than 0.60; thus, the lateral instability of the capsule was reduced. In fact, at $\theta_F \geq 60$ some lateral stability was noted. Although the capsule was laterally stable at $\theta_F = 86$, there was no indication of a trim point in the longitudinal plane. Again, it is not known what attitude the capsule would assume in the pitch plane. Data obtained with the BP_{31} configuration are presented in Fig. 13b. A stable trim point occurred near zero angle of attack for zero pressure ratio; however, with the jet on no trim point was evident. At this Mach number, as was the case at Mach number 0.60, the parachute was moving rapidly in the jet wake, and data at high angles of attack could not be obtained. The lateral stability of the capsule (BP_{31}) was quite good at zero jet pressure ratio. Unfortunately, data were not obtained with configuration BP_{31} using the jet in the yaw plane.*

*Although the balance was not capable of obtaining pitch and yaw data simultaneously, the model was yawed, and motion pictures were taken with the jet on. The results indicated violent parachute action at yaw angles greater than ±1 deg.

The lateral and longitudinal stability characteristics of configurations B and BP_{31} at Mach number 1.50 are presented in Fig. 14. The results obtained at Mach number 1.50 (see Fig. 14a) differed from those previously discussed at the lower Mach numbers in that as λ increased, with the stabilization frame folded (θ_F = -15), the axial-force coefficients decreased. When the stabilization frame was deployed to 20 deg, the jet impinged on the frame, as was the case at lower Mach numbers, and C_A increased as λ increased. Once the frame was out of the region of jet impingement, the axial-force coefficients again tended to decrease as λ increased. At Mach number 1.5 (Fig. 14a) the capsule was stable in the yaw plane for $\theta_F \geq 60$. Stable trim points in the longitudinal plane occurred when the frame was fully deployed.

Only a very limited amount of data was obtained with the parachute attached to the capsule (BP_{31}) at Mach number 1.5 (see Fig. 14b). The data presented for the parachute at $\lambda \sim 680$ are subject to considerable doubt because the parachute was highly unstable and exerted considerable dynamic forces on the model (and consequently, produced erratic balance outputs). In general, the stability characteristics of the capsule were better at Mach number 1.5 than at the two lower Mach numbers previously discussed.

Data obtained with the pilot capsule (B') are presented in Figs. 15, 16, and 17 for Mach numbers 0.60, 0.93, and 1.5, respectively. Generally, the results obtained with the pilot capsule were comparable to those of the crew capsule when the jet was not used. This was expected since the differences in body geometry were slight. However, the effect of the jet was considerably different for the two configurations because the thrust lines of the nozzles were different.

The effect of increasing λ on the lateral stability of the pilot capsule at several frame angles can be seen in Fig. 15. The most pronounced effects of λ occurred when the frame was partially deployed (θ_F = -4). With the frame at this angle, the jet impinged on the left-hand yaw fin (looking upstream) and thus caused a large negative side-force acting aft on the capsule. The large negative side-force resulted in positive or unstable yawing-moment coefficients (Fig. 15a). There is no indication from the data that the configuration would trim until the stabilization frame angle approaches 86 deg. At θ_F = 86, if the data were extrapolated, the configuration would possibly trim in the lateral plane at a yaw angle between 25 and 30 deg. The results with the parachute ($B'P_{31}$) are presented in Fig. 15b for the stabilization frame fully deployed. Large positive pitching-moment and yawing-moment coefficients were experienced by the capsule when the jet was used. Again, as was the case for the crew capsule, the parachute reacted violently to the jet; consequently

only a limited amount of data was obtained. There was no clear indication from the results using the jet that the capsule would trim. However, it is felt that the capsule would assume a large positive angle of attack and would experience a large positive rolling moment during frame deployment because of the jet impingement on one fin.

At Mach number 0.93 the same trends occurred (Fig. 16a) as discussed for Mach number 0.60. However, at Mach number 0.93, the magnitude of the forces was somewhat smaller than shown for Mach number 0.60. With the stabilization frame angle at 86 deg, the pilot capsule had a stable trim point in the yaw plane at 8 and 25 deg for λ = 320 and 660, respectively (Fig. 16a). The yawing-moment coefficients (θ_F = 86) tended to coalesce at the higher yaw angles (λ = 320 and 660 as opposed to zero) because as the capsule was yawed in the positive direction, the wake from the jet was deflected away from the back of the capsule. As shown in Fig. 16b, the data for the pilot capsule with a parachute ($B'P_{31}$) indicated the probability of trimming at a yaw angle of about 10 deg at λ = 650. However, in the pitch plane, the data indicated the lack of a trim point at small angles of attack with the jet air simulation.

The stability characteristics of the pilot capsule at Mach number 1.5 are presented in Fig. 17. The capsule was unstable in the lateral plane with the jet operating until the stabilization frame approached 86 deg. The results indicated a stable trim point in the yaw plane at about 5 deg of yaw (Fig. 17b). In the pitch plane, the data indicated no tendency for the capsule to assume a trim condition with the highest jet pressure ratio. Again, the data were difficult to obtain when using the jet air simulation and parachute because of the rapid and violent movement of the parachute in the jet wake.

COMPARISON OF COLD AIR SIMULATION AND ROCKET FIRINGS

Several small-scale rocket motors were fired during one phase of the test in an attempt to determine the validity of the cold air simulation. The rocket chamber pressure for the small rockets was in the neighborhood of 500 psia in contrast to 2600 psia for the proposed full-scale rockets. Consequently, for a given pressure altitude, the pressure ratio, λ, for the small-scale rockets was one-fifth that of the large motors. Therefore, it was necessary to operate the wind tunnel at very low dynamic pressures to obtain realistic values of λ; thus, relatively small aerodynamic loads were produced on the model. To complicate further the interpretation of the data, the installation of the rockets in

the model necessitated the use of a balance with a high load-carrying capacity.* In most cases the forces experienced by the model as a result of the rocket firing were barely beyond the resolution of the balance. As mentioned previously, the balance outputs during the firings were recorded on an oscillograph. The determination of the model forces from the traces was difficult because the dynamic forces were superimposed on the static deflection between rocket off and the rocket firing. Therefore, the uncertainties shown in the figures are based on the ability to read the traces to within ±0.05 inch, which is felt to be a realistic reading error for these data.

A plot of λ for the full-scale rocket (based on chamber pressure of 2600 psia) as a function of altitude is shown in Fig. 18a. Also, a curve indicating the λ required for the air simulation to duplicate a jet boundary produced by the rocket is shown in Fig. 18b. This correlation was supplied by the capsule contractor and was based on work performed by Goethert and Barnes (Ref. 3). In general, altitudes between 16,000 and 36,000 ft were simulated with the cold air jet at the three test Mach numbers.

Comparisons of the results obtained with the cold air simulation and the rocket firings are presented in Figs. 19 and 20 for Mach numbers 0.93 and 1.50, respectively. The one predominant fact apparent from the figures is that the forces exerted on the capsule during the rocket firings were lower than or equal to those encountered with the air jet simulation. Moving the rocket data points to a lower value of λ, as shown in Fig. 18b, did not significantly improve the correlation when the uncertainties are considered. In general, the results were not conclusive, and more rocket firings are needed to clearly establish trends. Rockets with much higher chamber pressures are required to produce realistic values of λ at higher values of free-stream dynamic pressure. Figure 18 indicates that the majority of rocket data points correspond to an altitude of approximately 25,000 ft. If the trends in the static stability characteristics persist in the manner indicated, then it is expected that the capsule will show a higher degree of instability as λ is increased to correspond to higher altitudes. However, the degree of instability tended to decrease as the Mach number was increased for a fixed value of λ. It should be mentioned that the parachute was pulled into the wake produced by the rocket motors in the same manner as experienced during the cold air simulation. However, the parachute movements were not as violent as those encountered during the air simulation which may be explained by the short burning time of the rockets (~ 2.0 sec).

---

*The balance was the only one available that would fit the model installation with the rocket installed.

CONCLUSIONS

The following conclusions were derived from a static stability investigation of the crew and pilot capsules for the B-58 aircraft at Mach numbers 0.60, 0.93, and 1.50:

1. In general, both the crew and pilot capsules showed a lack of static stability in the lateral and longitudinal planes with an indication of stable trim points only at large angles of attack and yaw.
2. The parachute attached to the capsule dipped violently in and out of the jet wake. This action produced large positive pitching-moment coefficients on the capsule.
3. The results obtained with small-scale rocket motors installed in the crew capsule were inconclusive. However, rocket motor operation appeared to produce less effect on the capsule aerodynamics than the cold air simulation.

REFERENCES

1. Test Facilities Handbook, (3rd Edition). "Propulsion Wind Tunnel Facility, Vol. 3." Arnold Engineering Development Center, January 1961.
2. Dean, R. C., Jr. Aerodynamic Measurements. Gas Turbine Laboratory, Massachusetts Institute of Technology, Cambridge, Massachusetts, 1953.
3. Goethert, B. H. and Barnes, L. T. "Some Studies of the Flow Pattern at the Base of Missiles with Rocket Exhaust Jets." AEDC-TR-58-12 (Revised), June 1960.

TABLE I

PARACHUTE NOMENCLATURE

Designation	Canopy Description	Area, ft^2	Porosity, percent	Shroud Line Length, ft	Trailback Distance, ft
P_{11}	Equiflow	0.694	24	0.937	6.59
P_{12}	Equiflow	1.042	24	1.146	6.59
P_{13}	Equiflow	1.389	24	1.324	6.59
P_{14}	Equiflow	0.694	24	1.873	6.59
P_{15}	Equiflow	0.694	24	0.937	5.28
P_{16}	Equiflow	0.694	24	0.937	7.90
P_{21}	Conical	1.111	24	1.188	6.59
P_{22}	Conical	1.042	20	1.146	6.59
P_{23}	Conical	1.042	18	1.146	6.59
P_{31}	Hemisflow	1.042	21	2.292	6.90

NOTE: All dimensions model scale

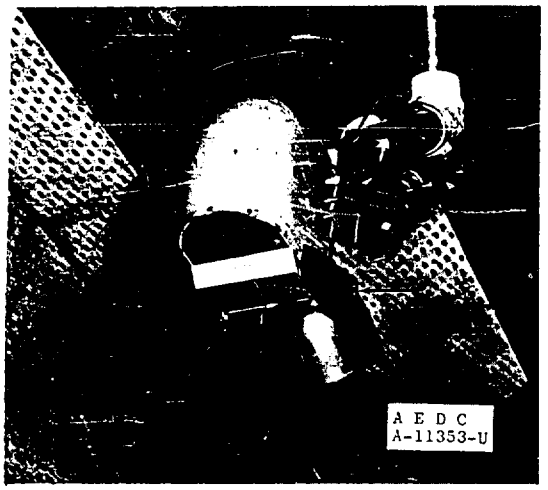

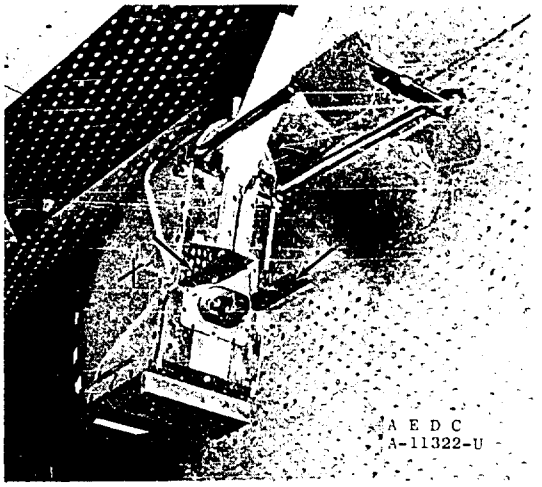

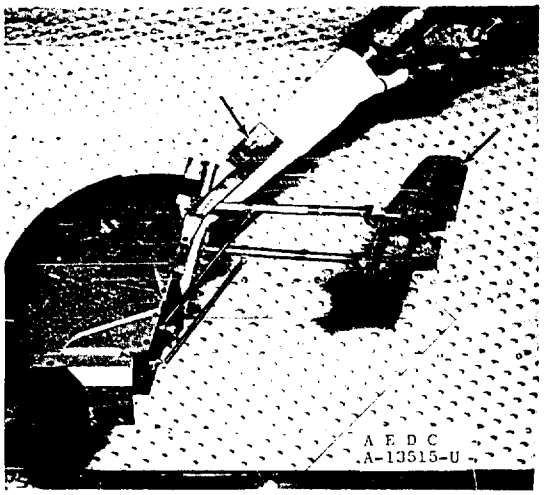

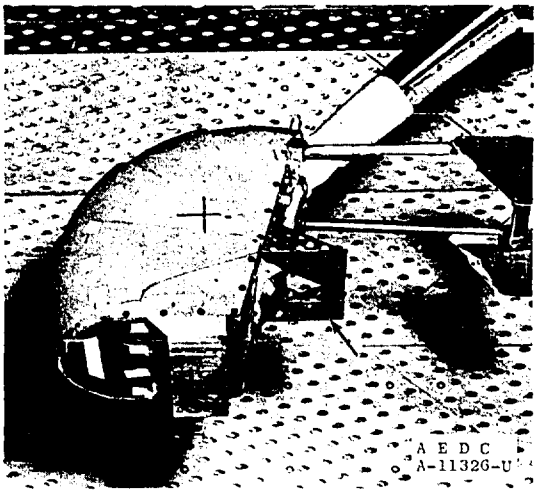

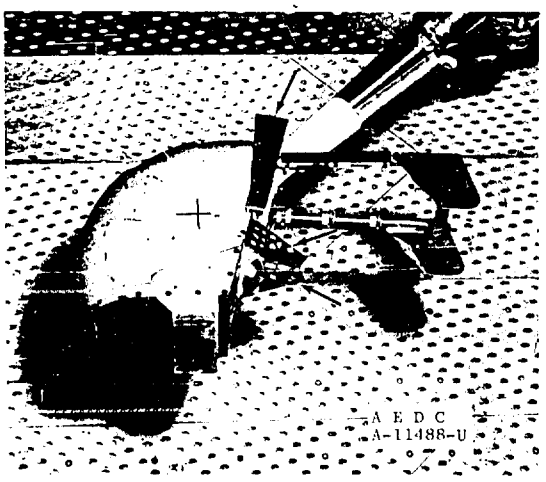

Arrows indicate modification to crew capsule.

Fig. 1 Photographs Indicating Some of the External Surfaces Added to the Crew Capsule

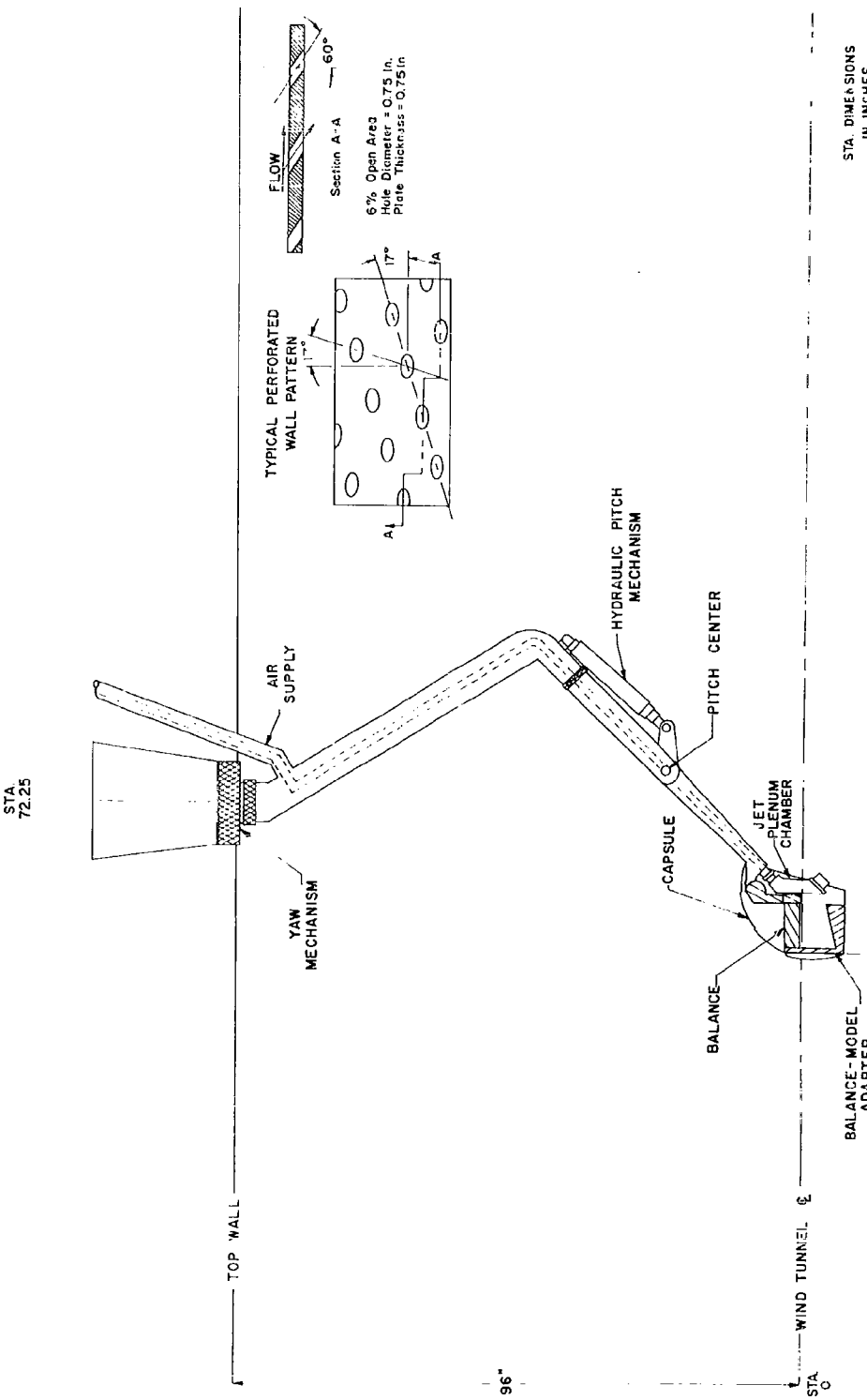

Fig. 2 Schematic Drawing of Test Installation

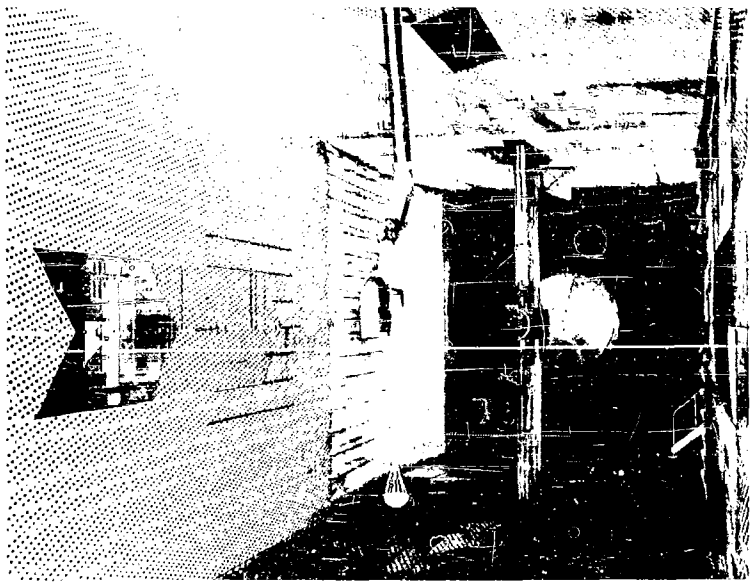

a. Front View

b. Rear View

Fig. 3 Typical Test Installation Photographs (Configuration BP_{11})

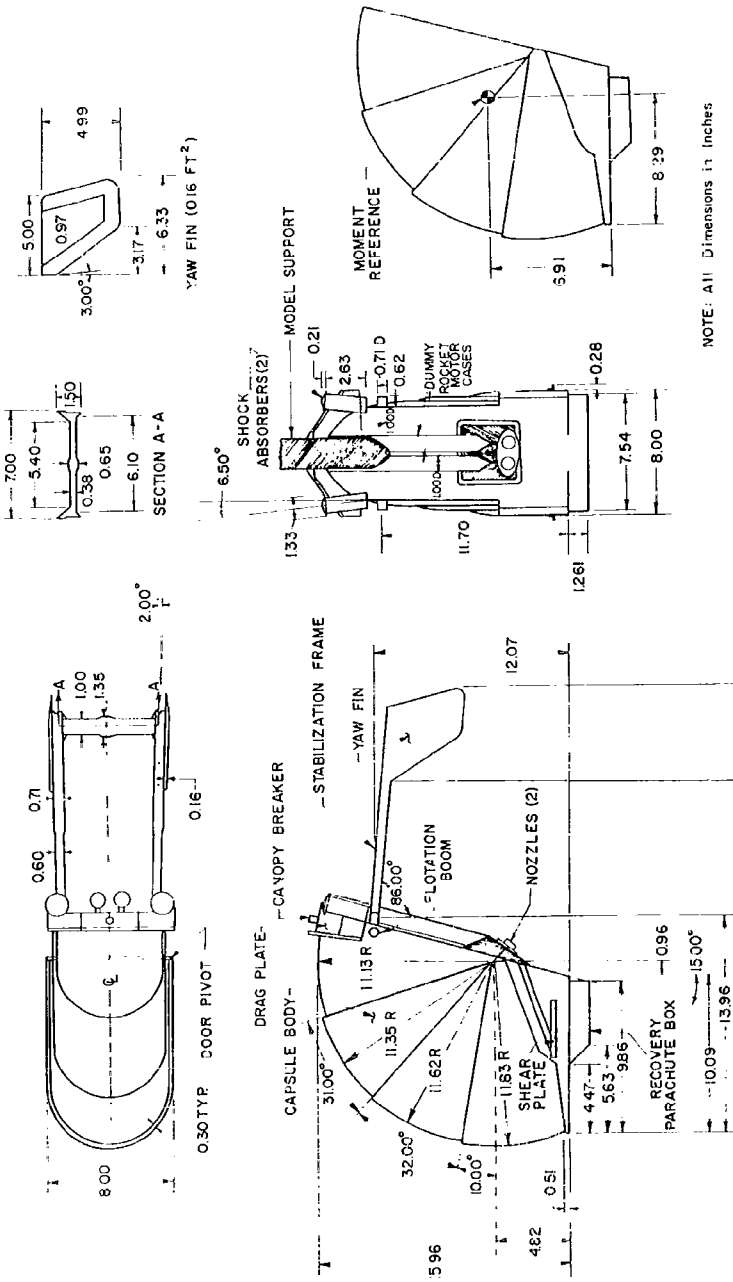

a. General Details

Fig. 4 Model Details and Dimensions

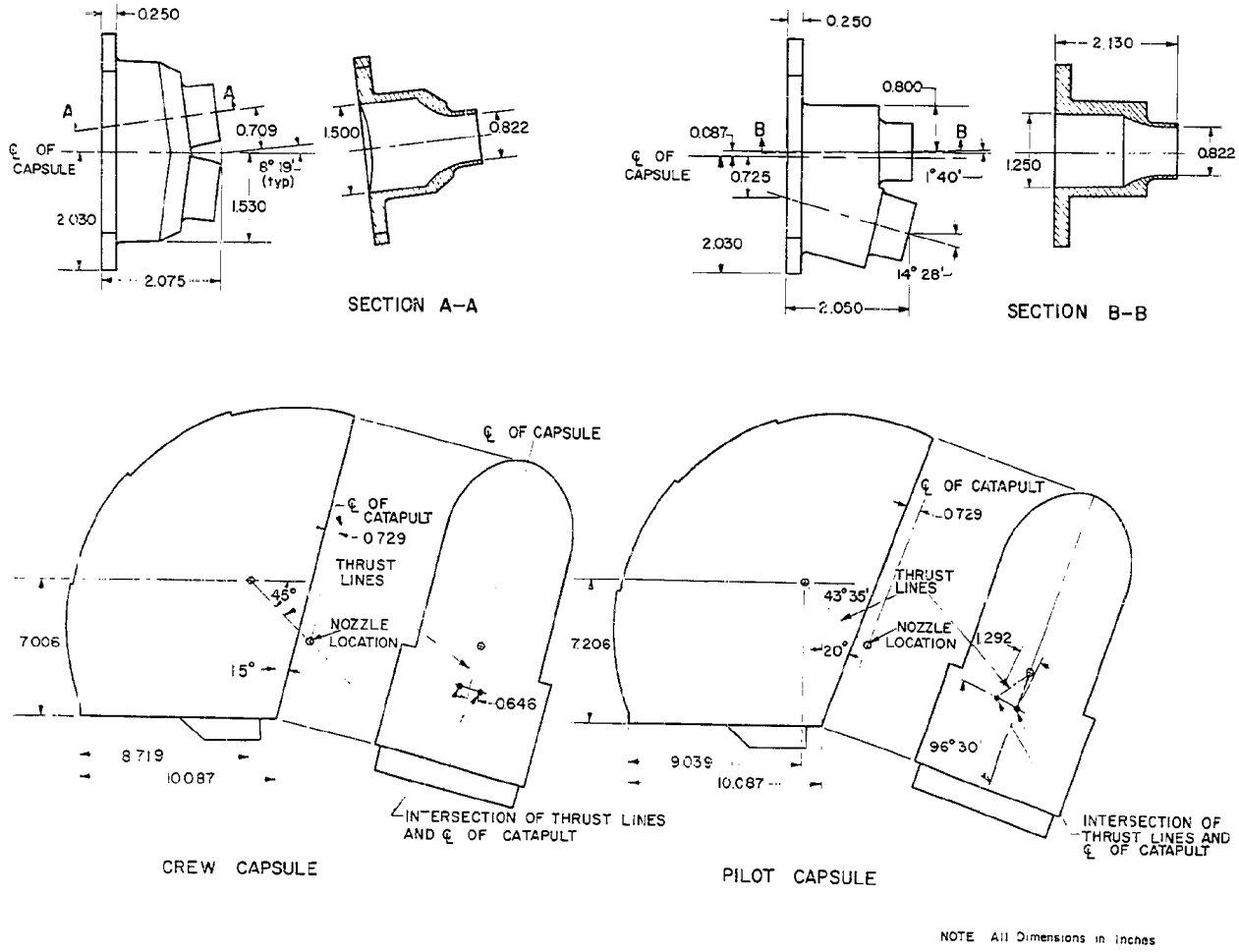

b. Jet Nozzle Details

Fig. 4 Concluded

a. Crew Capsule (B)

Fig. 5 Installation Photographs Showing General Capsule Components

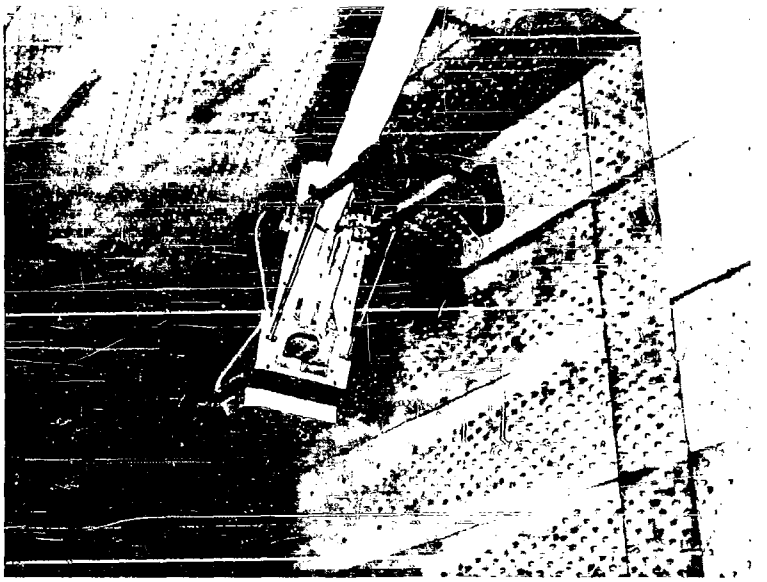

b. Pilot Capsule (B′)

c. Crew Capsule (B) Indicating Rocket Motor Installation

Fig. 5 Continued

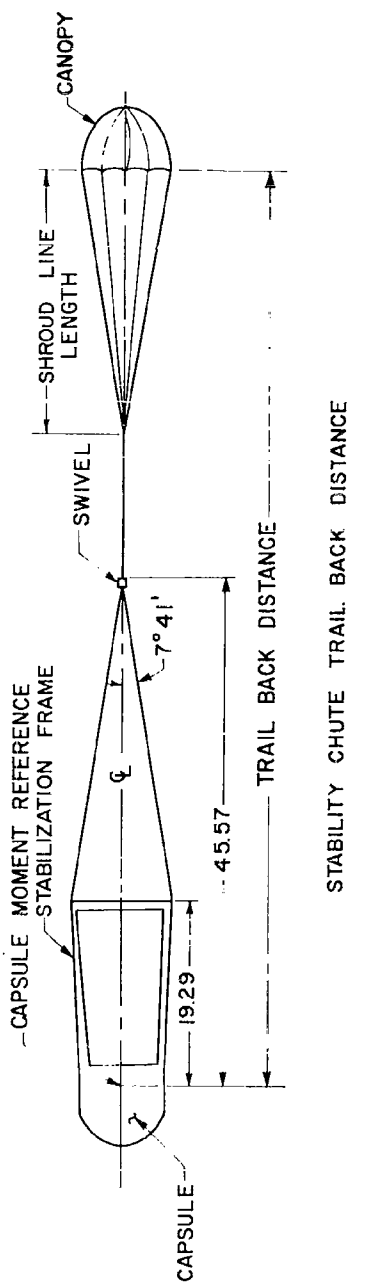

STABILITY CHUTE TRAIL BACK DISTANCE

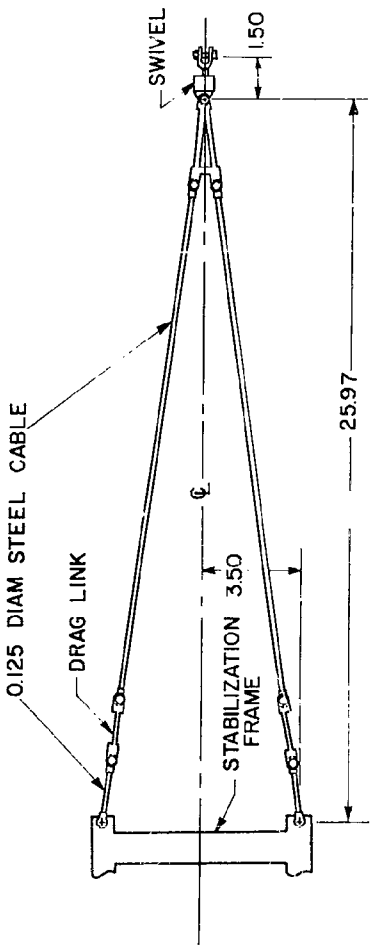

BRIDLE AND DRAG LINK ASSEMBLY

NOTE: All Dimensions in Inches

Fig. 6 General Drawing of the Parachute Assembly

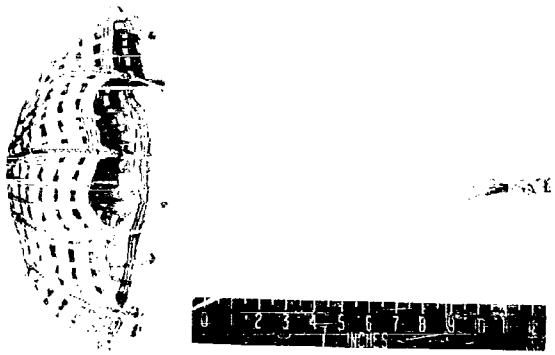

a. Conical

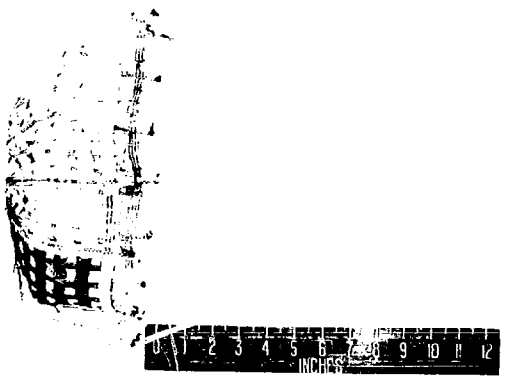

b. Equiflow

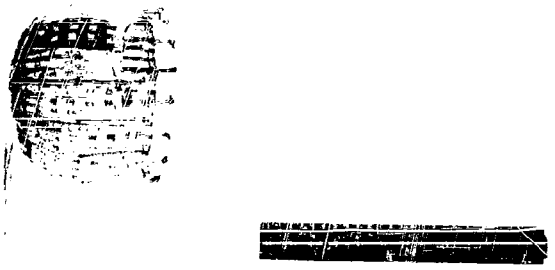

c. Hemisflow

Fig. 7 Photographs of the Three Types of Parachute Canopies Investigated

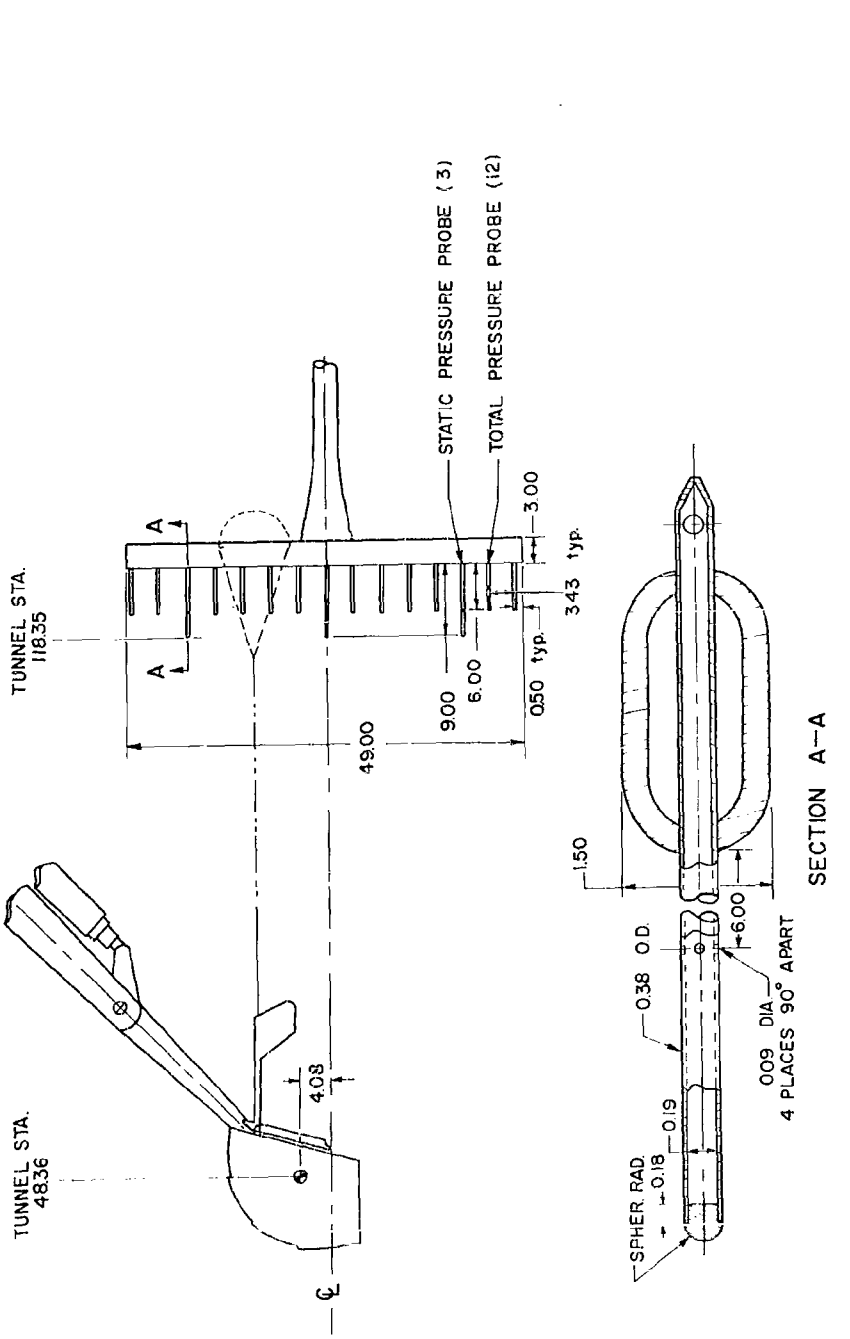

NOTE: All Dimensions in Inches

Fig. 8 Details and Location in the Test Section of the Wake Survey Rake

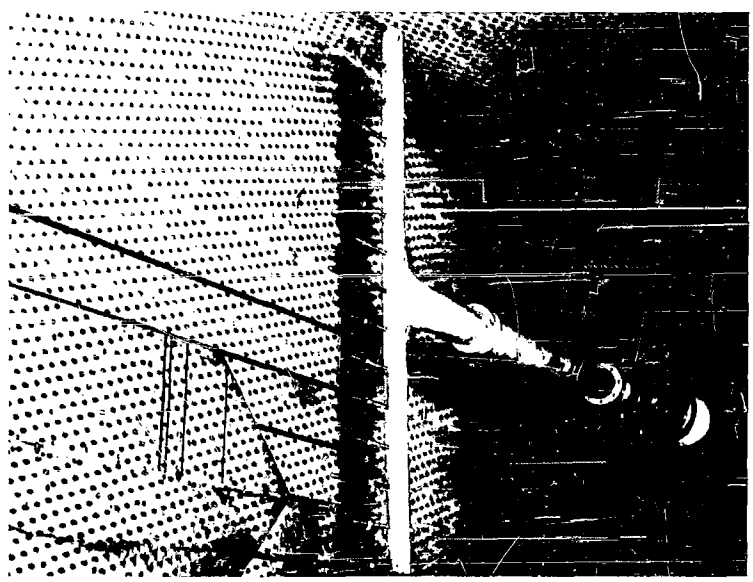

Fig. 9 Installation Photograph of the Wake Survey Rake

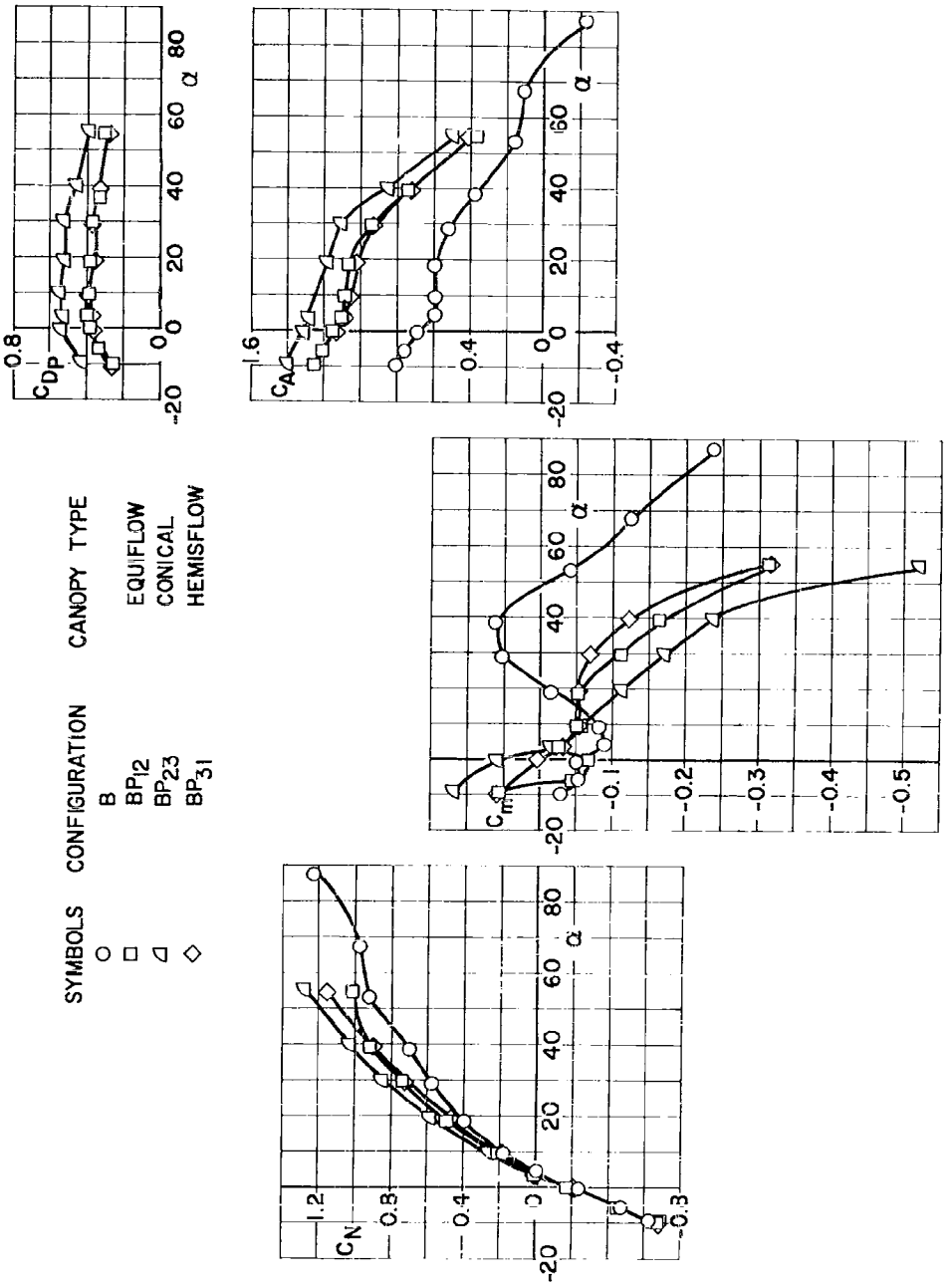

a. Canopy Configuration

Fig. 10 The Influence of Several Parachute Parameters on Parachute Drag and Crew Capsule (B) Aerodynamics at Mach Number 0.93 and a Reynolds Number of Approximately 1.2 Million

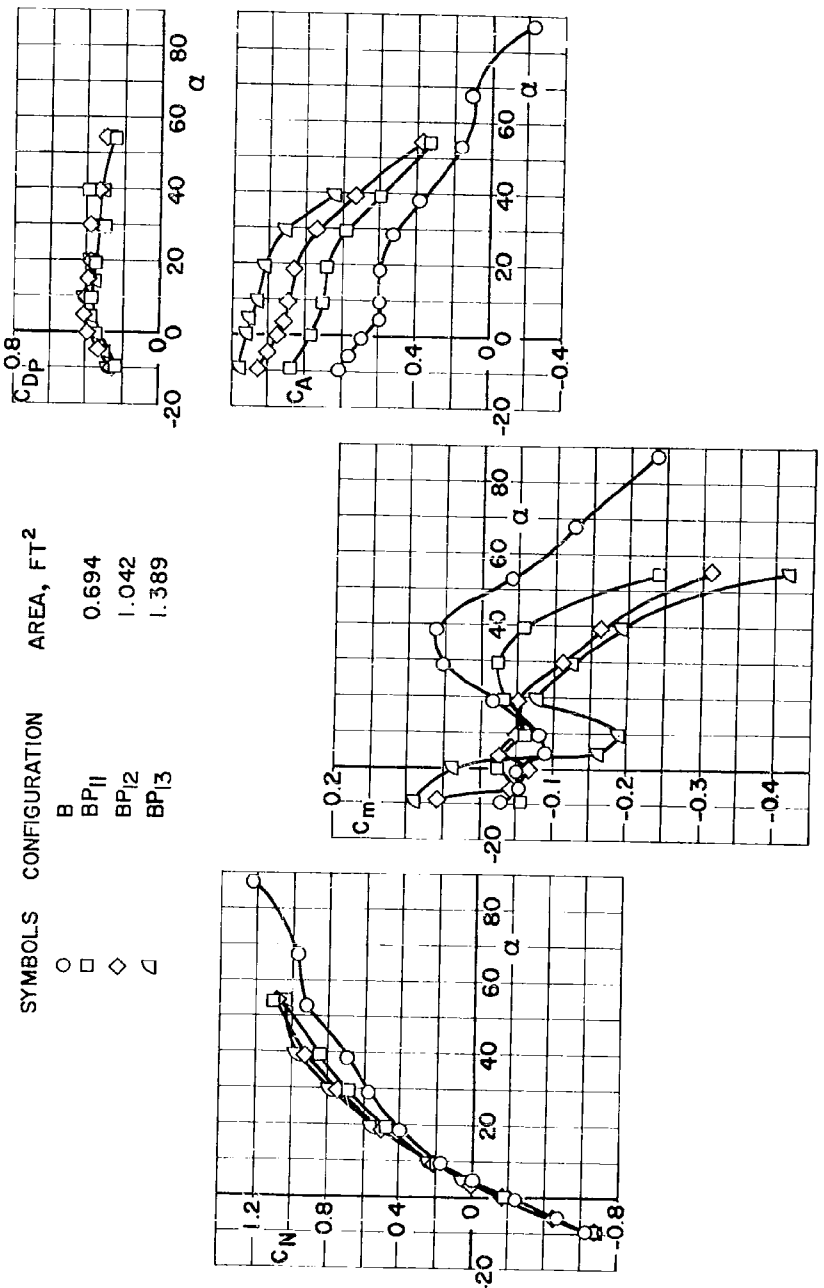

b. Parachute Area

Fig. 10 Continued

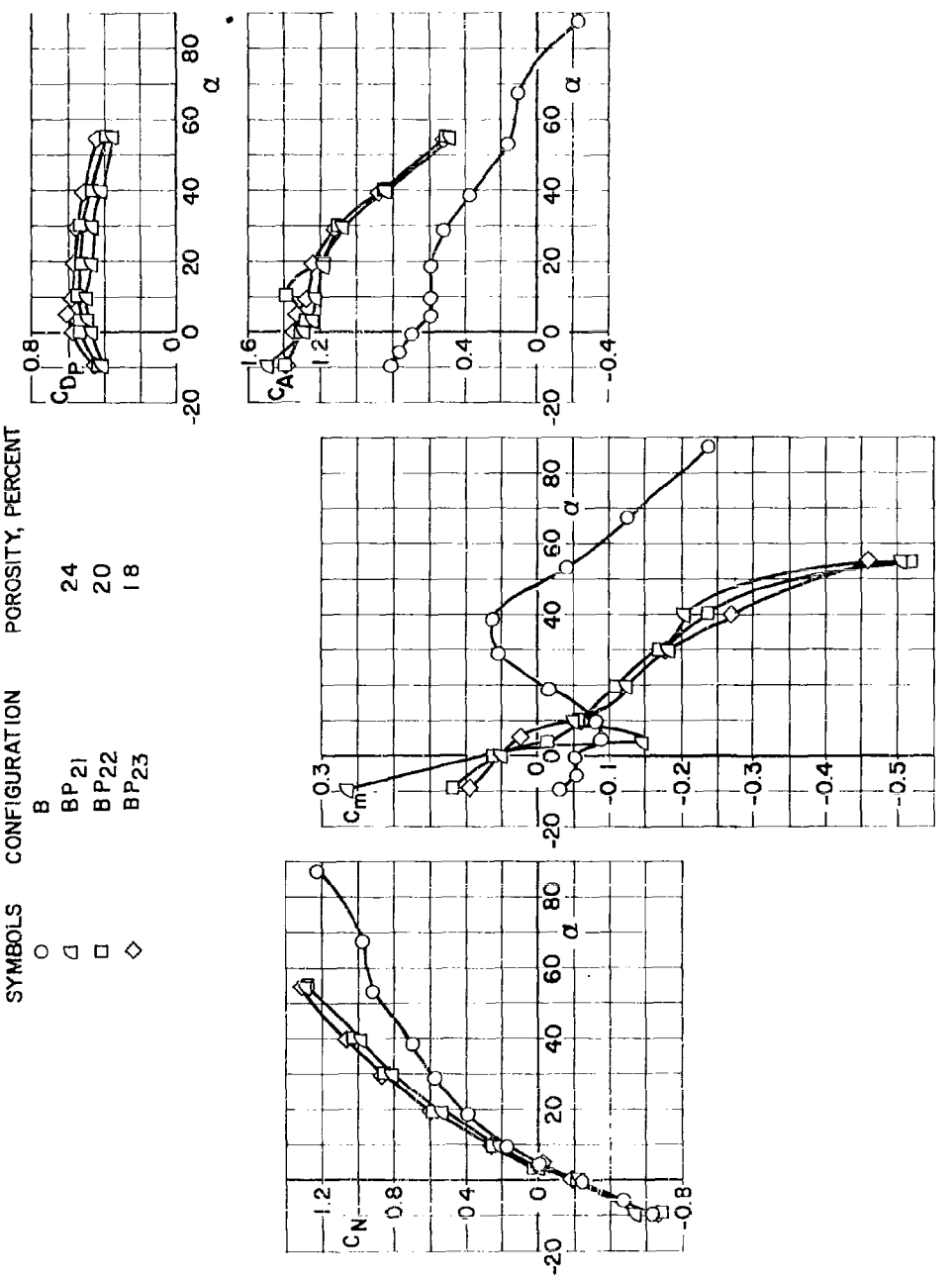

c. Parachute Porosity

Fig. 10 Continued

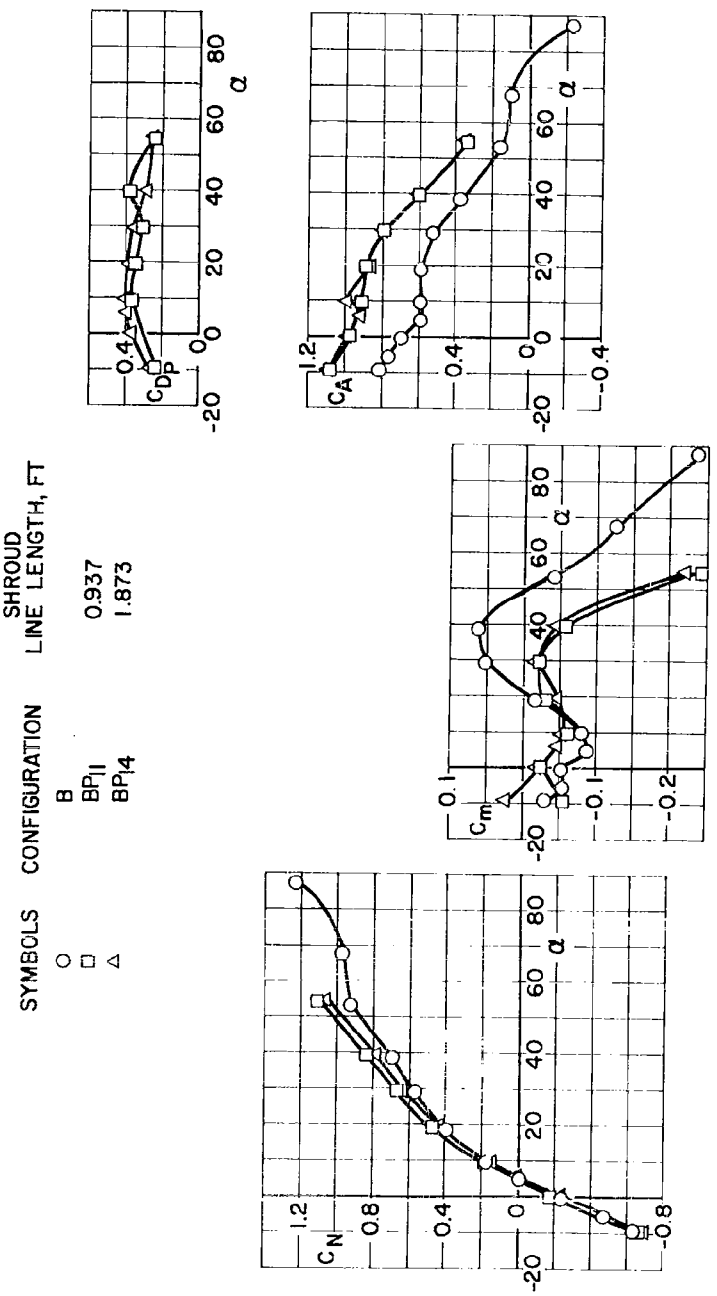

d. Shroud Line Length

Fig. 10 Continued

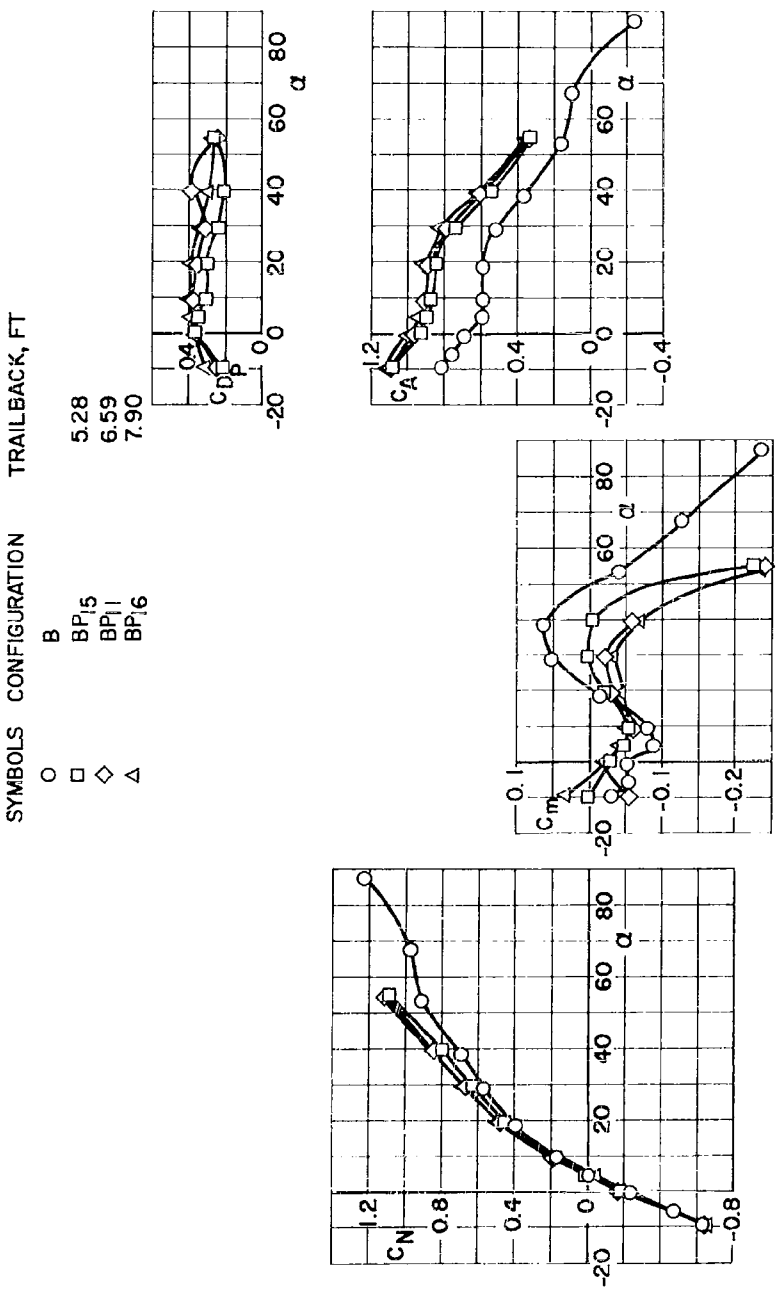

e. Trailback Distance

Fig. 10 Concluded

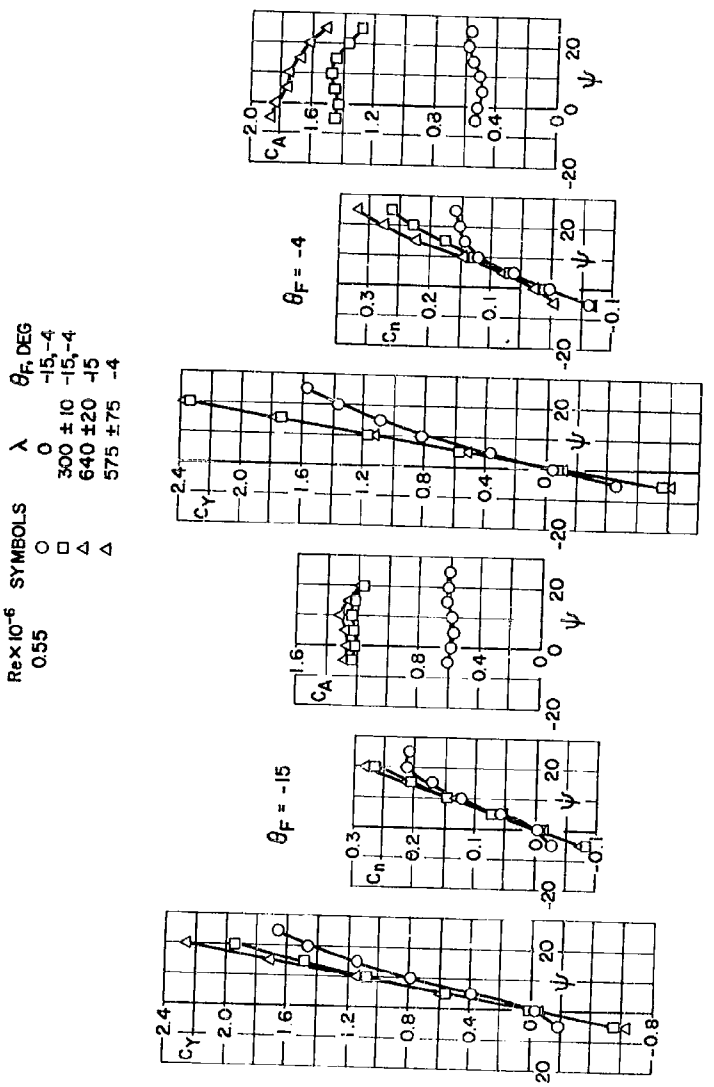

a. Configuration B

Fig. 11 Lateral and Longitudinal Stability Characteristics at Mach Number 0.60 for the Crew Capsule with Several Values of Jet Pressure Ratio and Stabilization Frame Angle

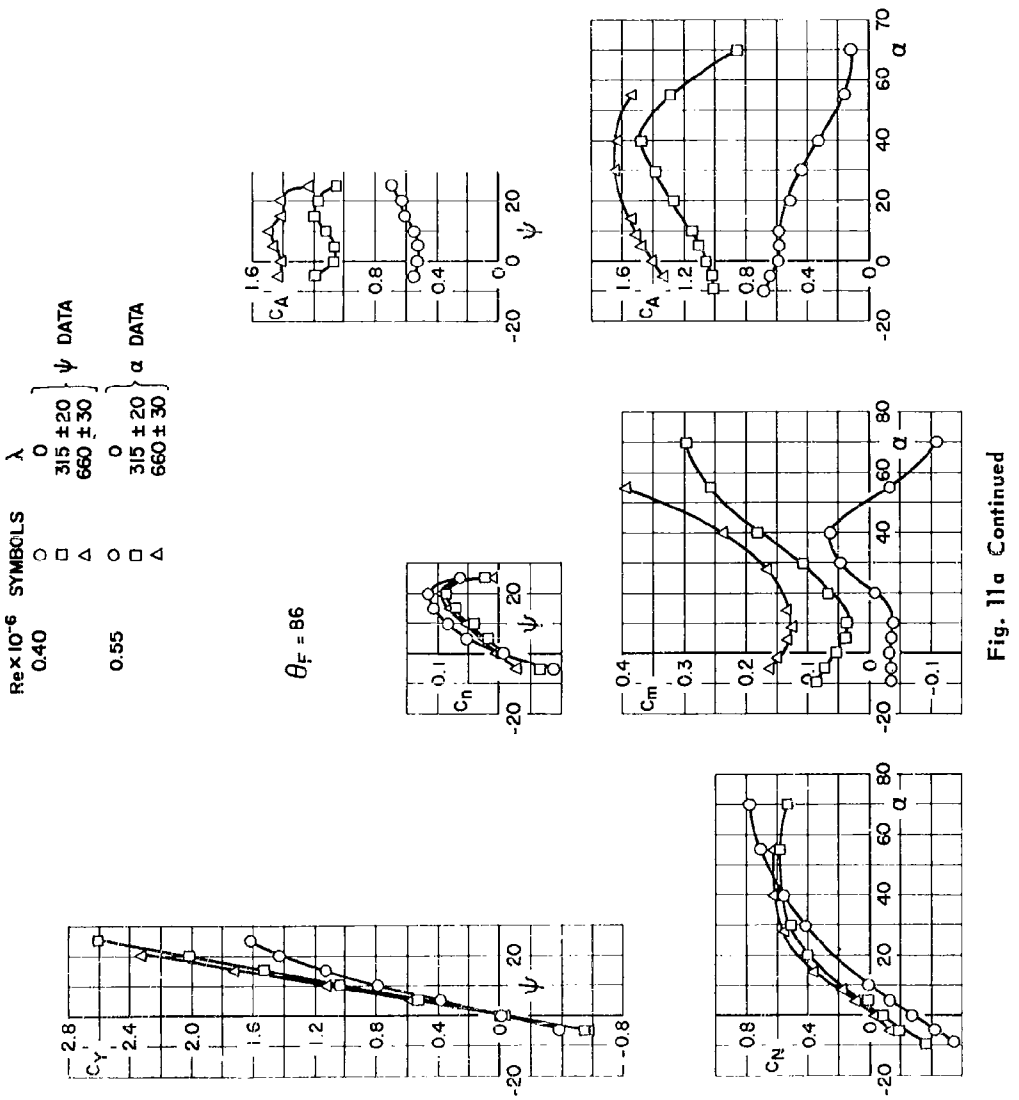

Fig. 11a Continued

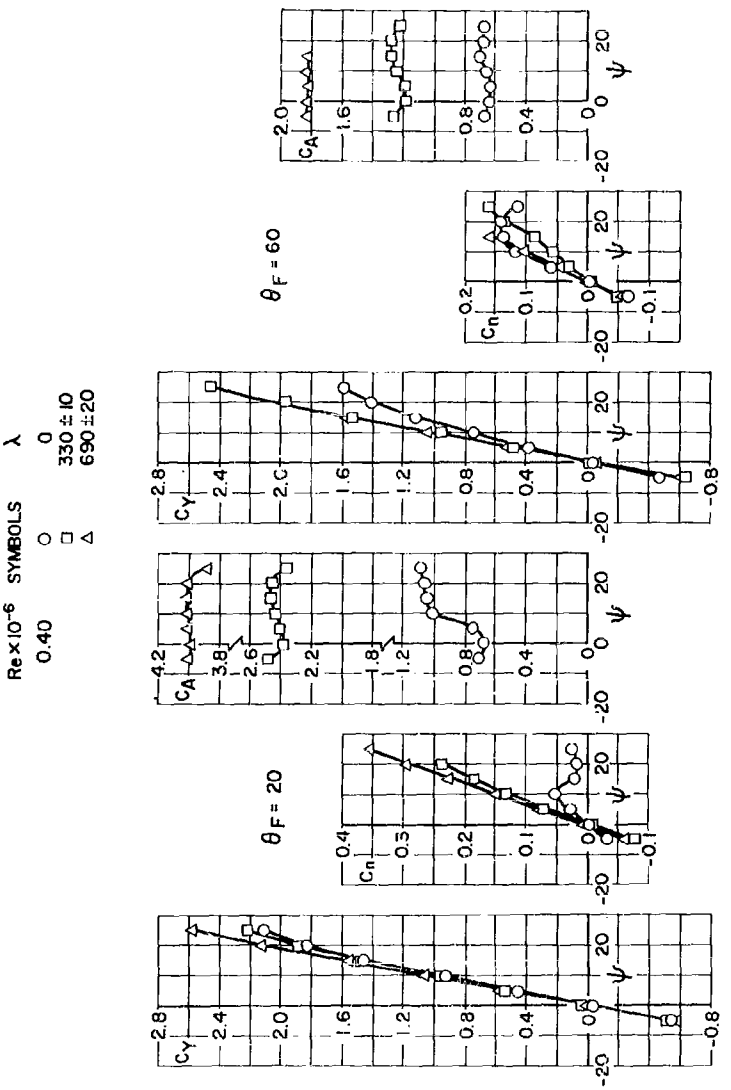

Fig. 11a Concluded

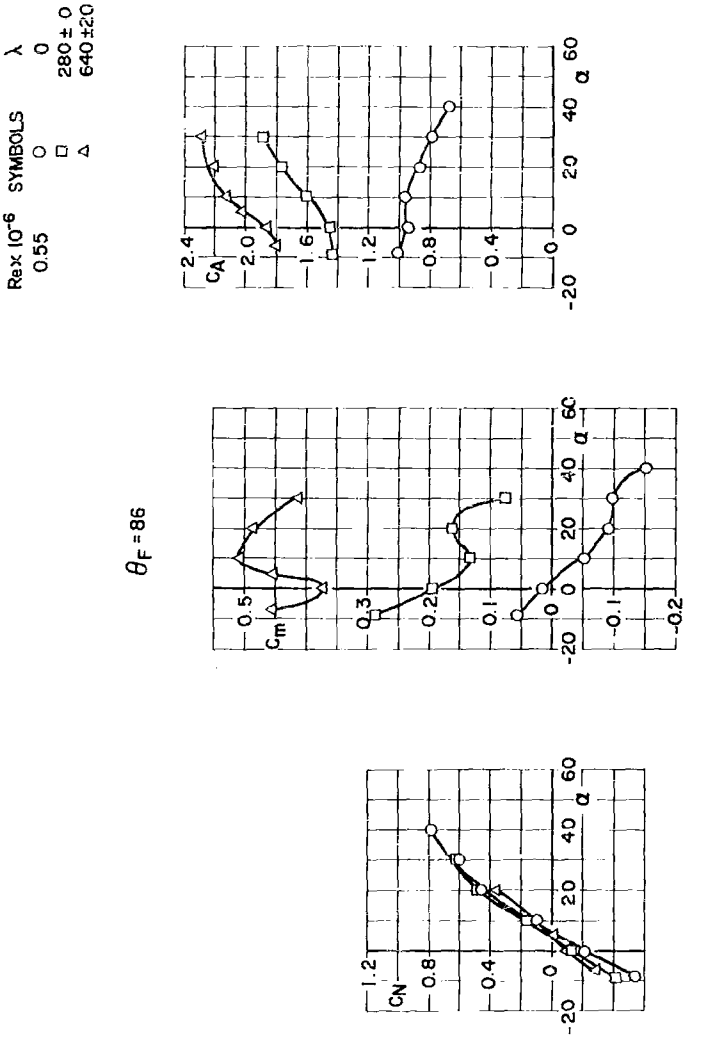

b. Configuration BP_{31}

Fig. 11 Concluded

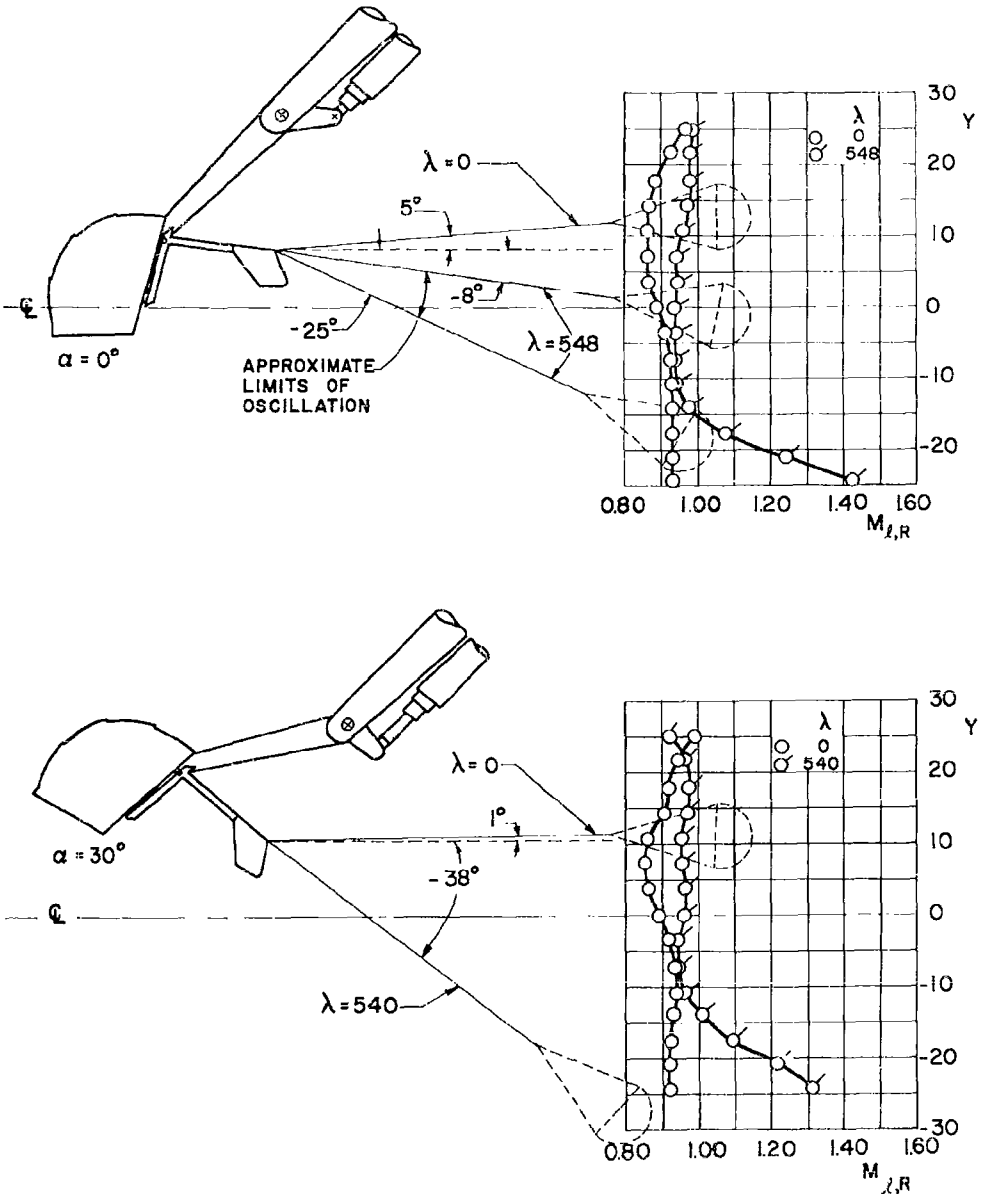

a. Vertical Mach Number Distribution

Fig. 12 Effect of Jet Pressure Ratio on the Capsule Wake in the Vicinity of the Parachute at Mach Number 0.93

$\lambda = 0$

$\lambda \sim 545$

$\lambda \sim 545$

b. Photographs Indicating the Parachute Movement

Fig. 12 Concluded

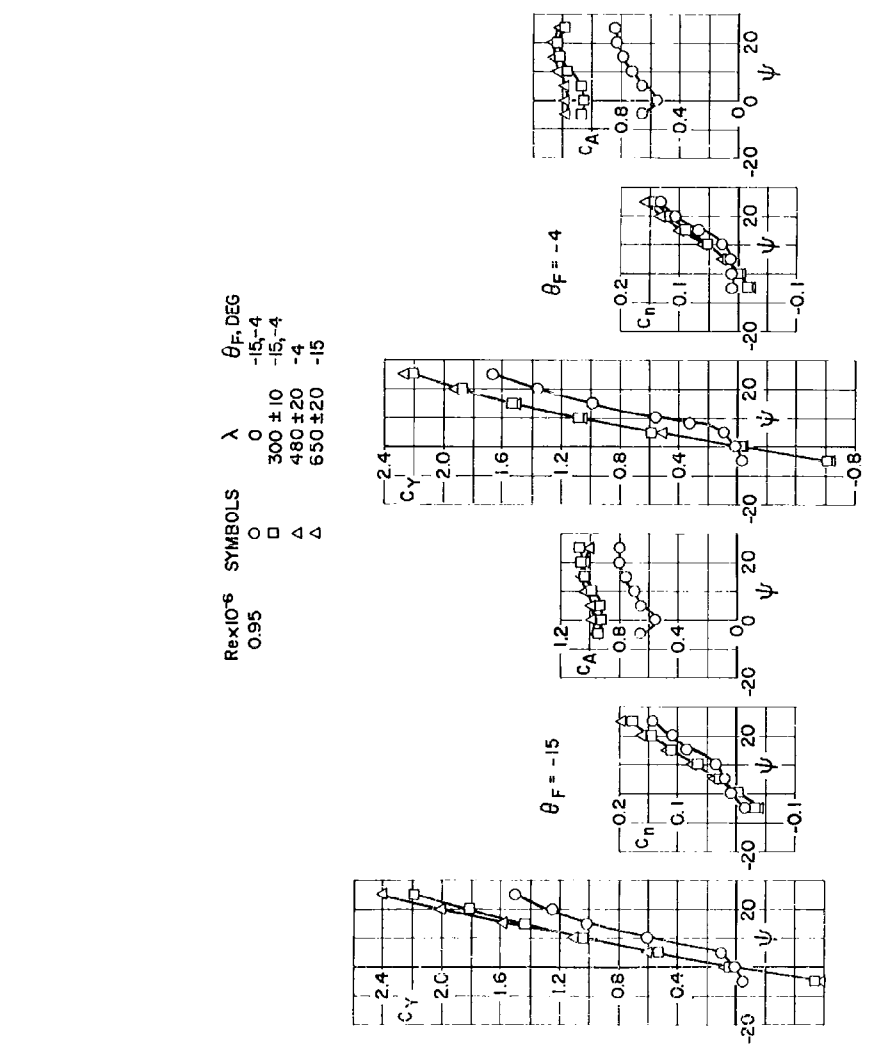

a. Configuration B

Fig. 13 Lateral and Longitudinal Stability Characteristics at Mach Number 0.93 for the Crew Capsule with Several Values of Jet Pressure Ratio and Stabilization Frame Angle

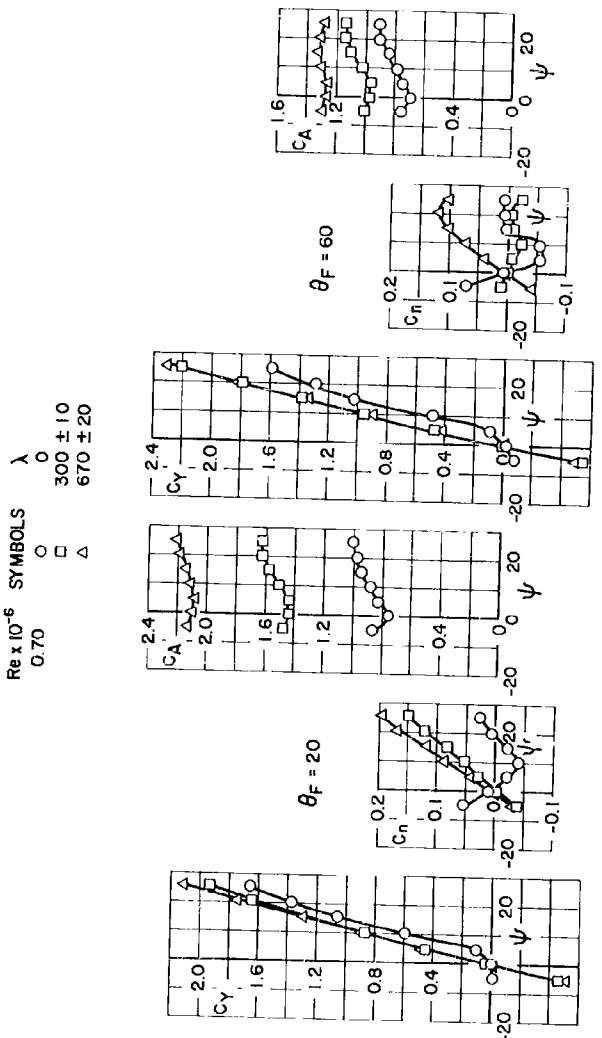

Fig. 13a Continued

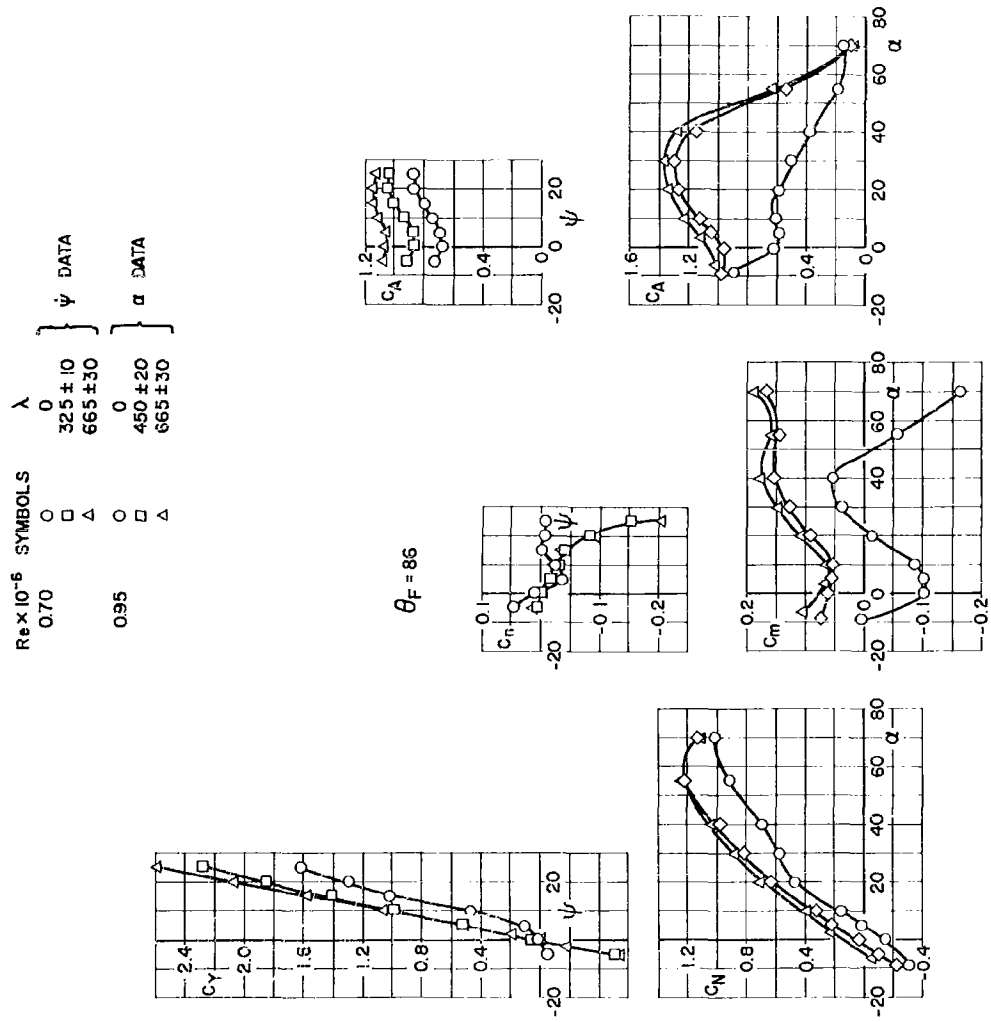

Fig. 13a Concluded

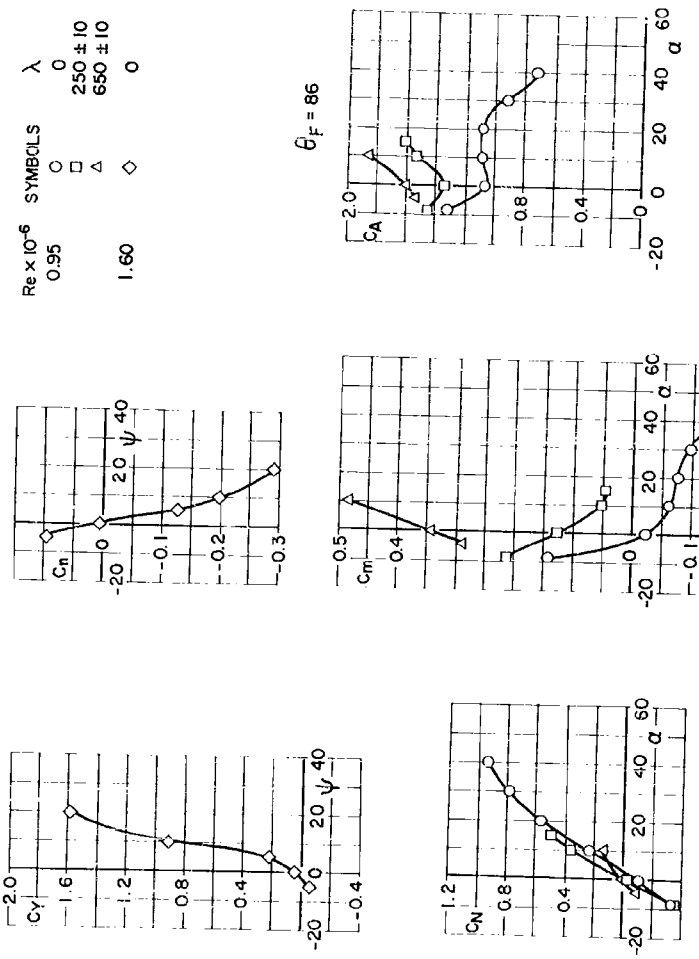

b. Configuration BP_{31}

Fig. 13 Concluded

Rex10^{-6}	SYMBOLS	λ	θ_F, DEG
2.20	○	0	-15, -4
	□	310 ± 10	-15
	△	620 ± 30	-15
1.32	○	0	20, 60
	□	330 ± 10	20, 60
	△	620 ± 40	20, 60

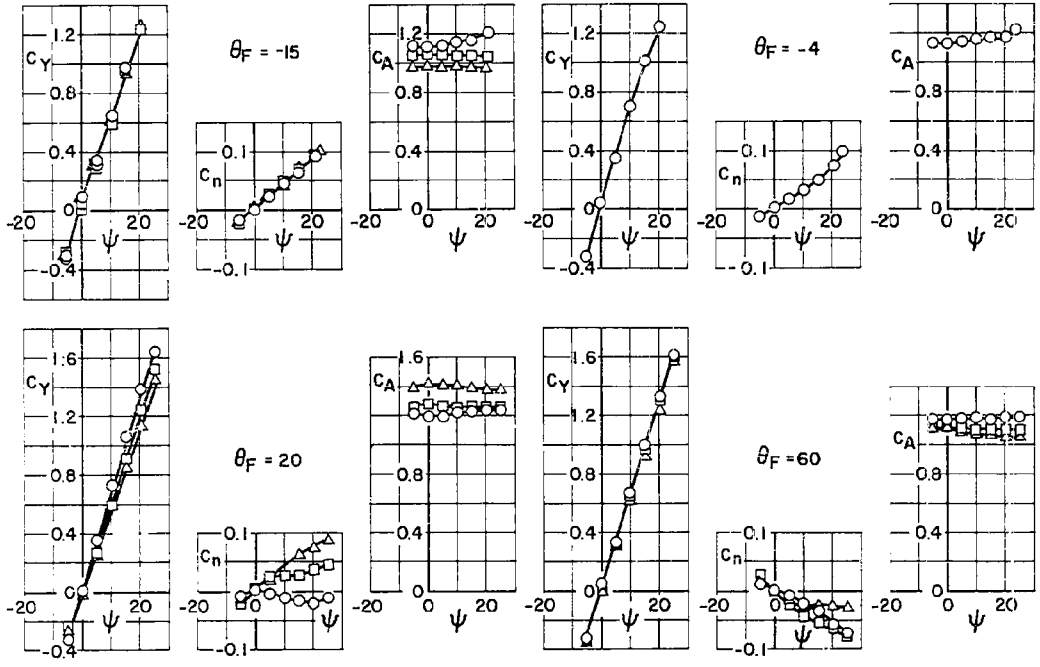

a. Configuration B

Fig. 14 Lateral and Longitudinal Stability Characteristics at Mach Number 1.50 for the Crew Capsule with Several Values of Jet Pressure Ratio and Stabilization Frame Angle

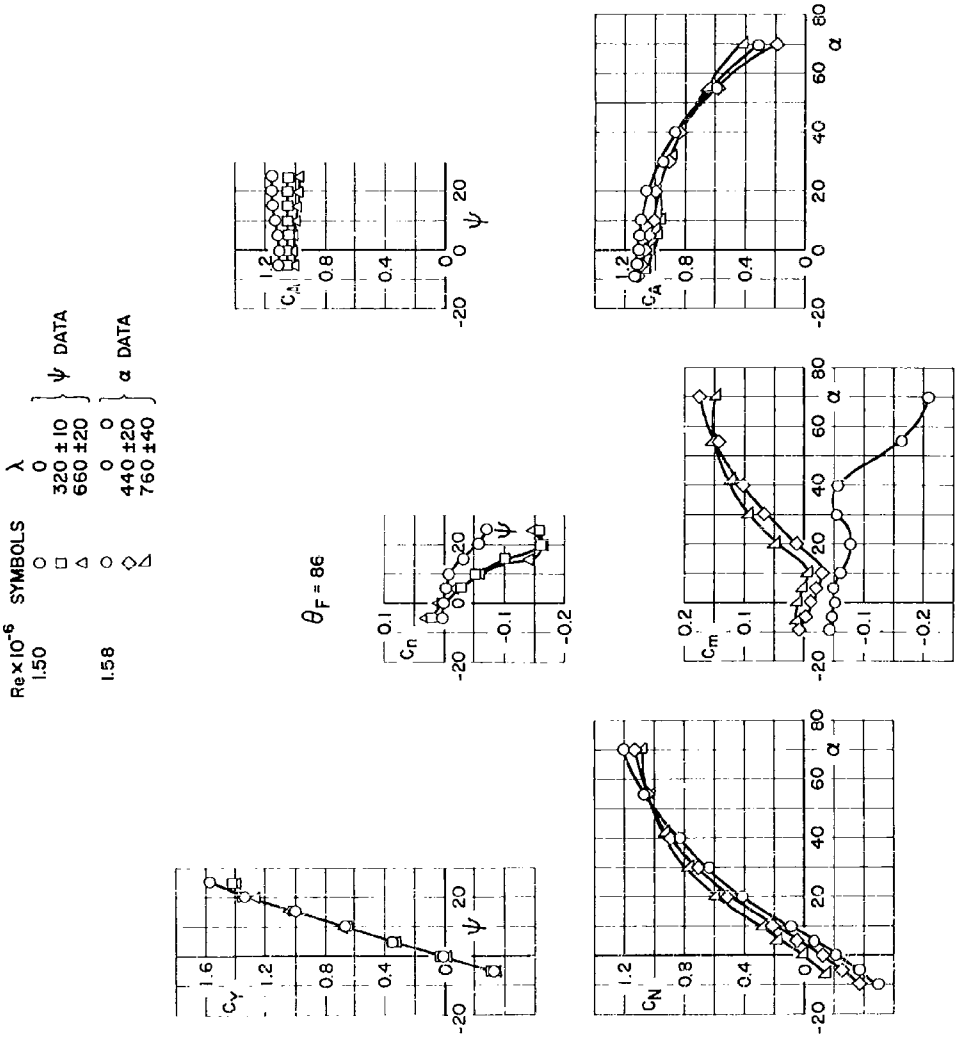

Fig. 14a Concluded

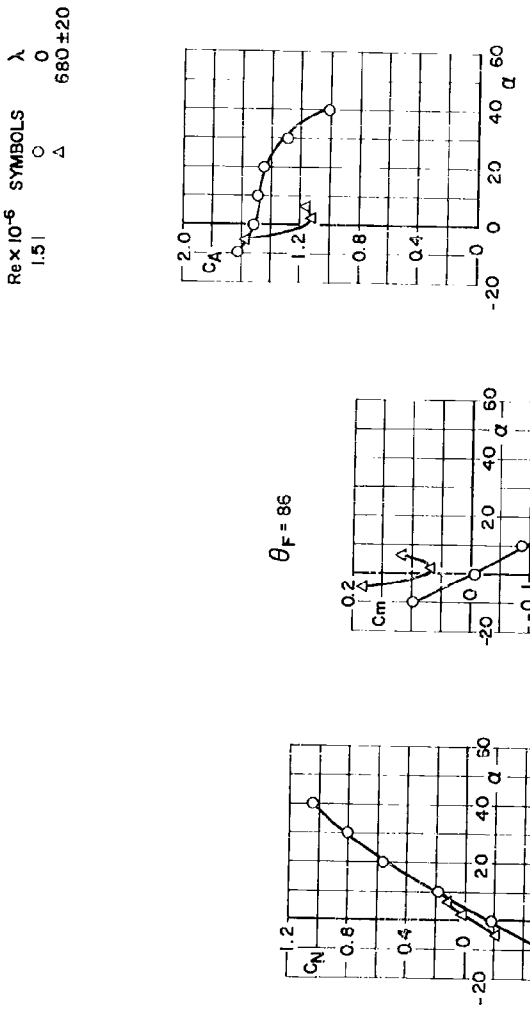

b. Configuration BP_{31}

Fig. 14 Concluded

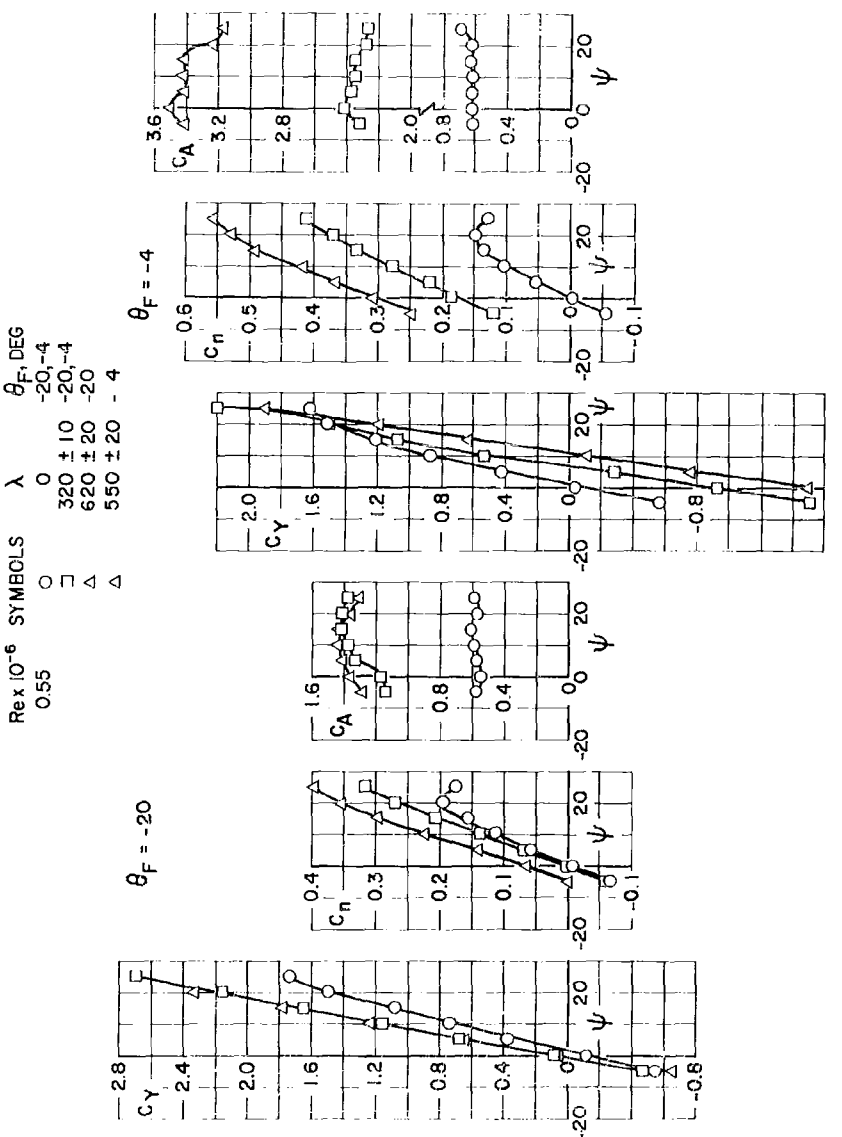

a. Configuration B′

Fig. 15 Lateral and Longitudinal Stability Characteristics at Mach Number 0.60 for the Pilot Capsule with Several Values of Jet Pressure Ratio and Stabilization Frame Angle

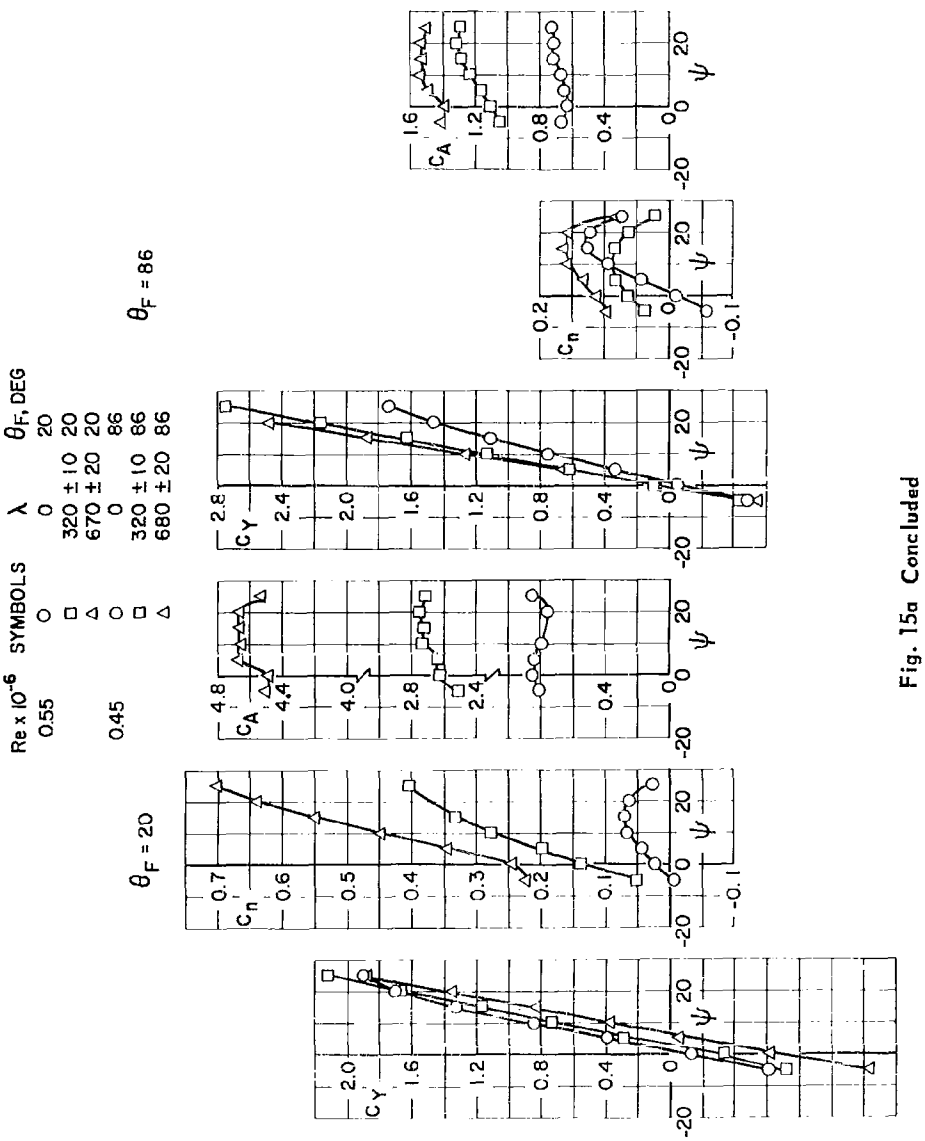

Fig. 15a Concluded

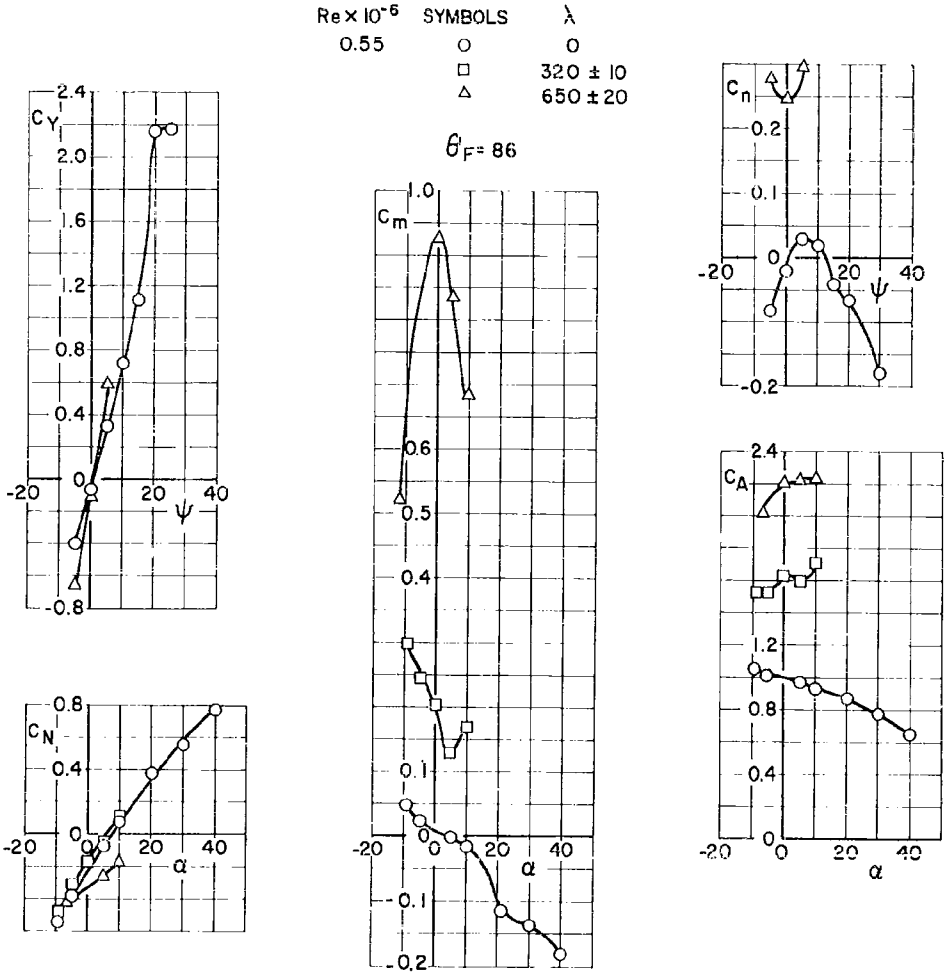

b. Configuration B´P31

Fig. 15 Concluded

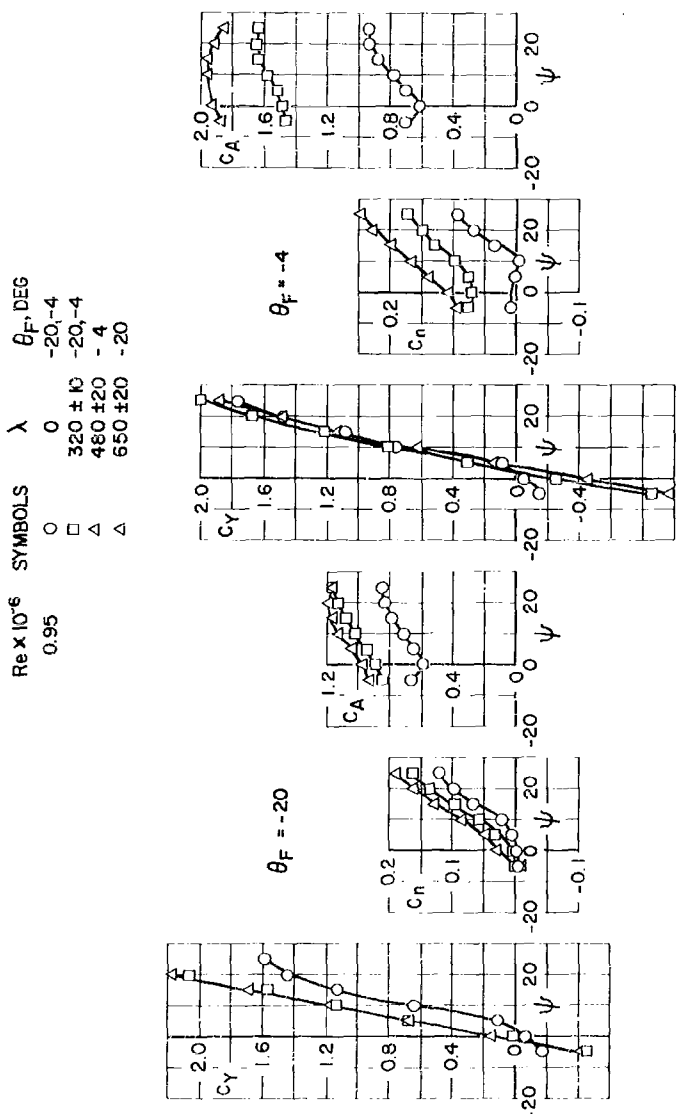

a. Configuration B′

Fig. 16 Lateral and Longitudinal Stability Characteristics at Mach Number 0.93 for the Pilot Capsule with Several Values of Jet Pressure Ratio and Stabilization Frame Angle

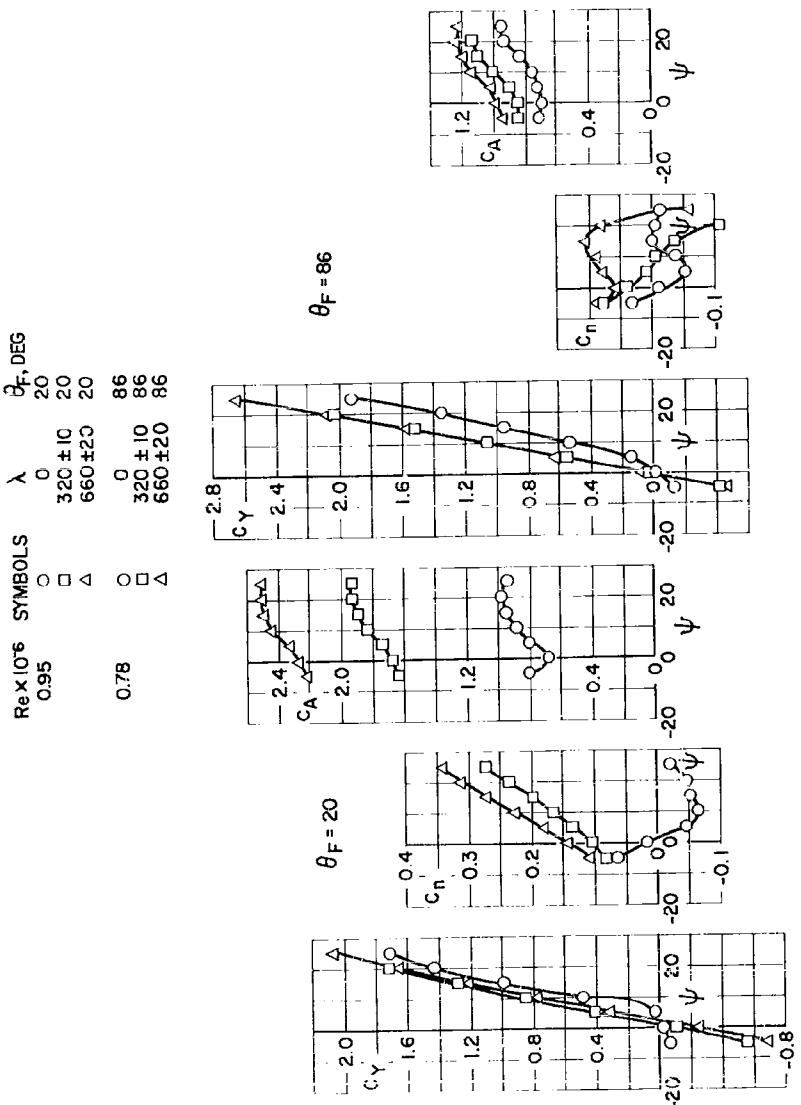

Fig. 16a Concluded

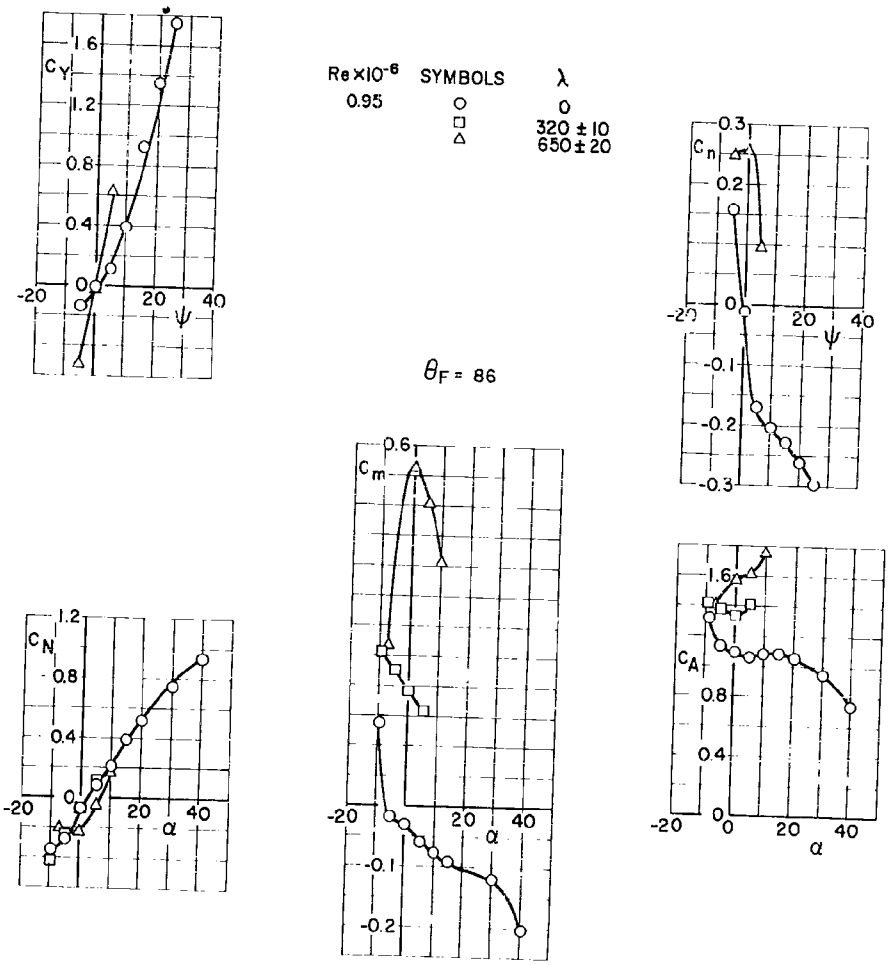

b. Configuration B′P31

Fig. 16 Concluded

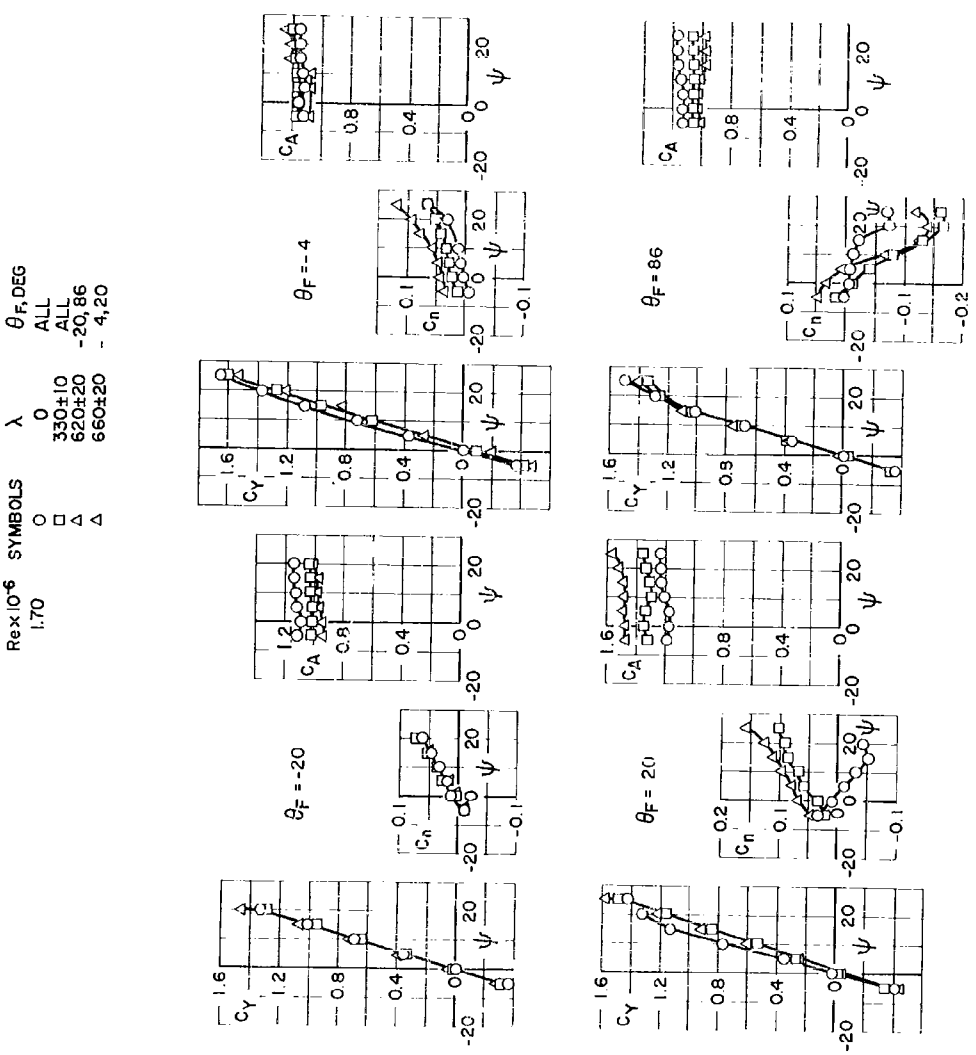

a. Configuration B'

Fig. 17 Lateral and Longitudinal Stability Characteristics at Mach Number 1.50 for the Pilot Capsule with Several Values of Jet Pressure Ratio and Stabilization Frame Angle

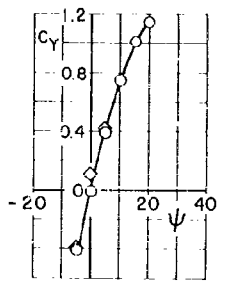

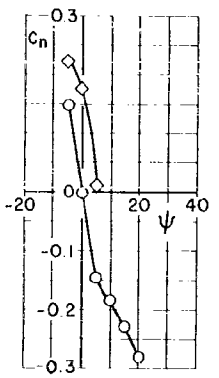

Re×10⁻⁶	SYMBOLS	λ
1.52	○	0
	□	360 ± 20
	◇	670 ± 20
	△	780 ± 20

$\theta_F = 86$

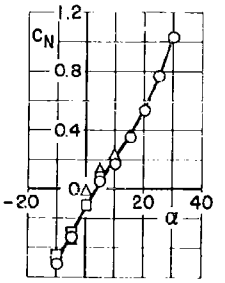

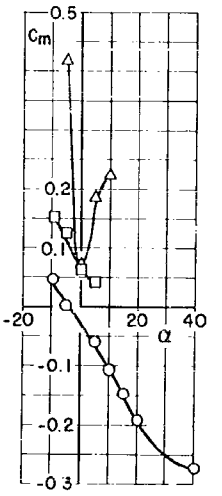

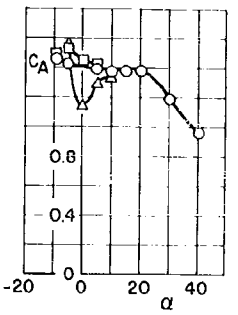

b. Configuration B′P_{31}

Fig. 17 Concluded

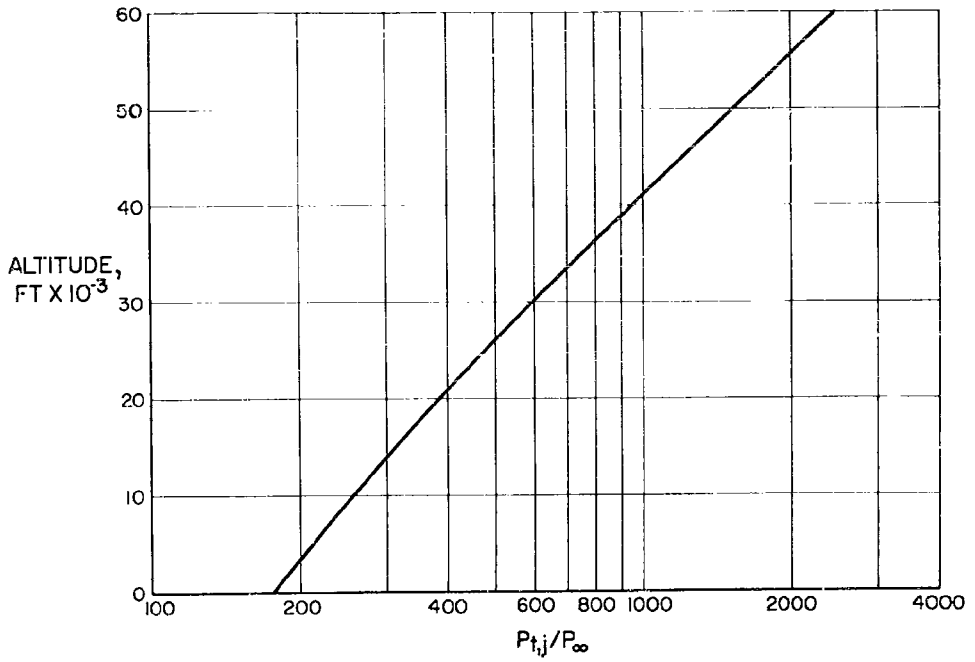

a. λ_{Rocket} as a Function of Altitude

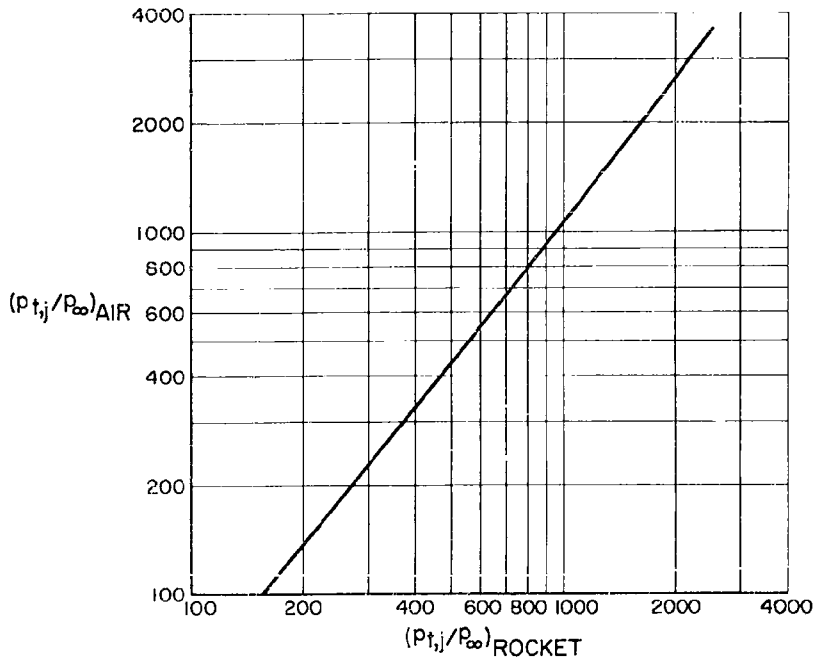

b. $\lambda_{Cold\ Air}$ as a Function of λ_{Rocket}

Fig. 18 Full-Scale Rocket Pressure Ratio (Based on $p_{t,j}$ Rocket = 2600 psia) as a Function of Altitude and a Correlation of Cold Air Pressure Ratio Required to Simulate Rocket Jet

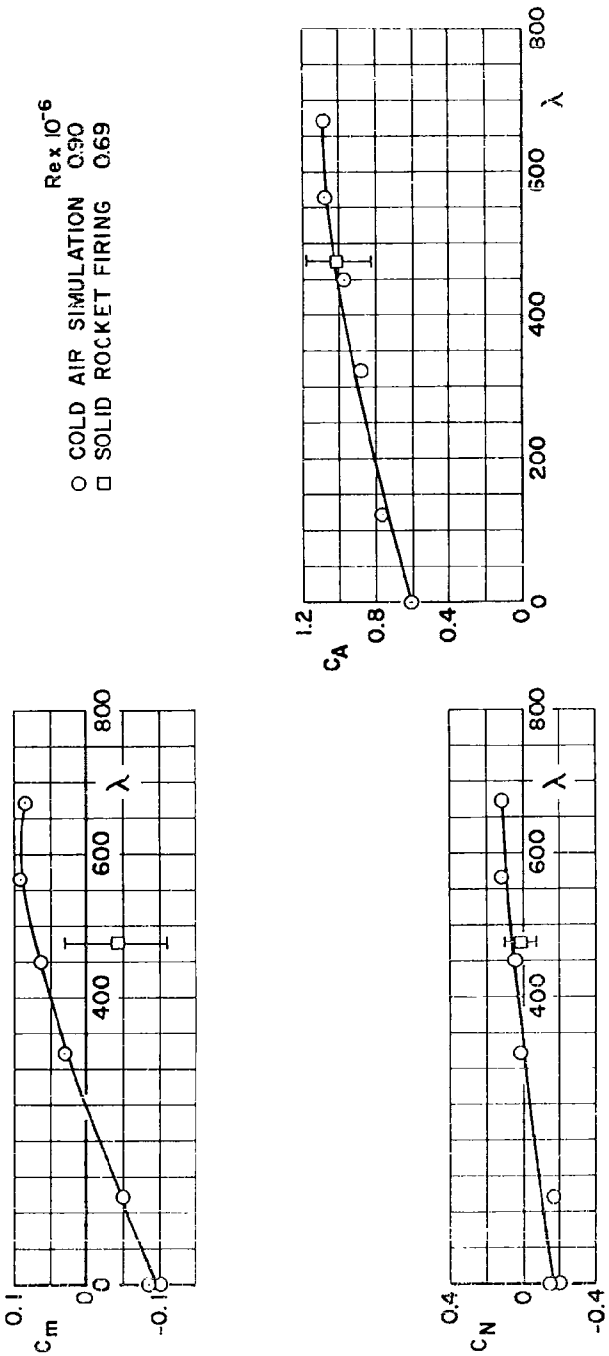

a. Crew Capsule (B) at Zero Angle of Attack

Fig. 19 Aerodynamic Coefficients for the Crew Capsule as a Function of Jet Pressure Ratio and Comparison with Rocket Firings at Mach Number 0.93

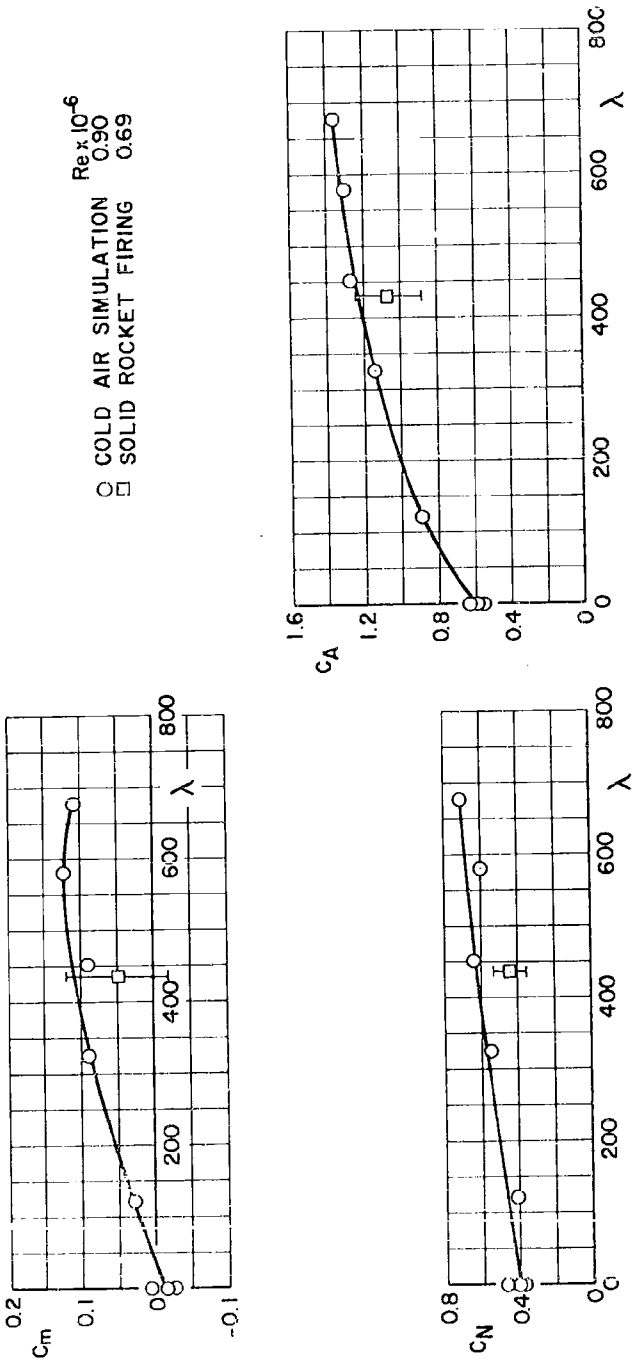

b. Crew Capsule (B) at 20-Deg Angle of Attack

Fig. 19 Continued

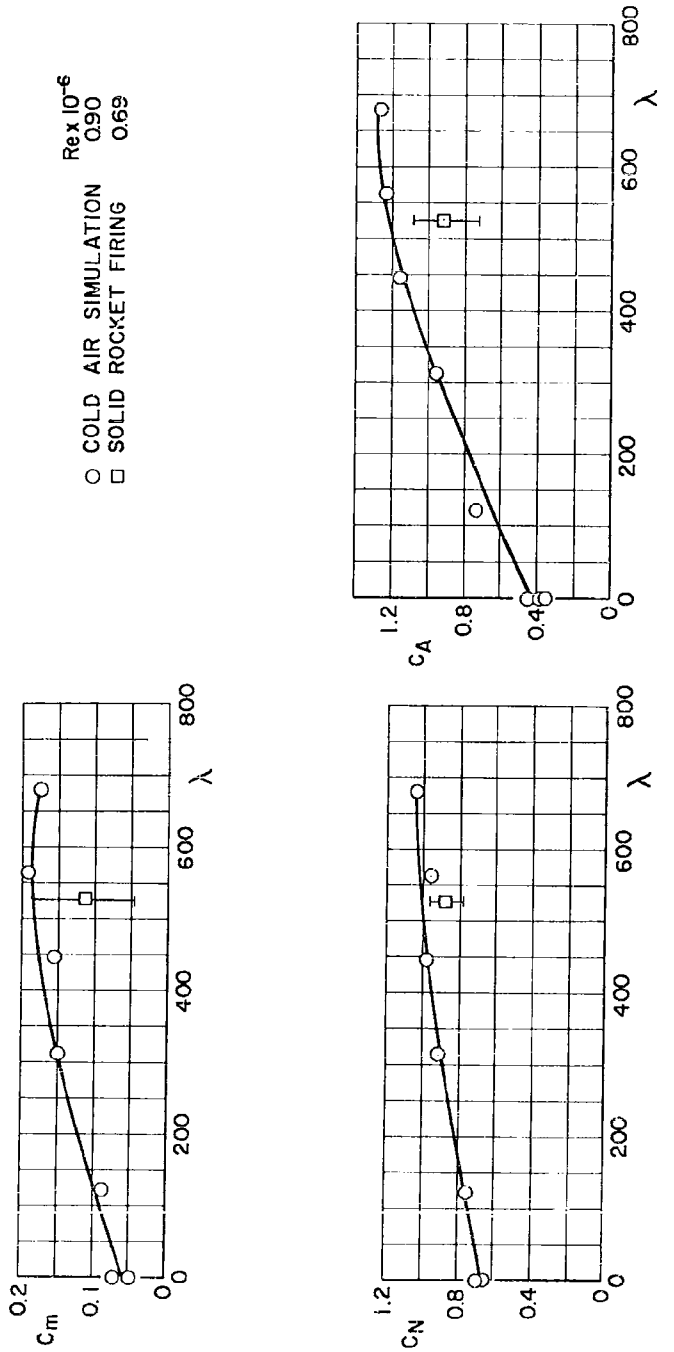

c. Crew Capsule (B) at 40-Deg Angle of Attack

Fig. 19 Continued

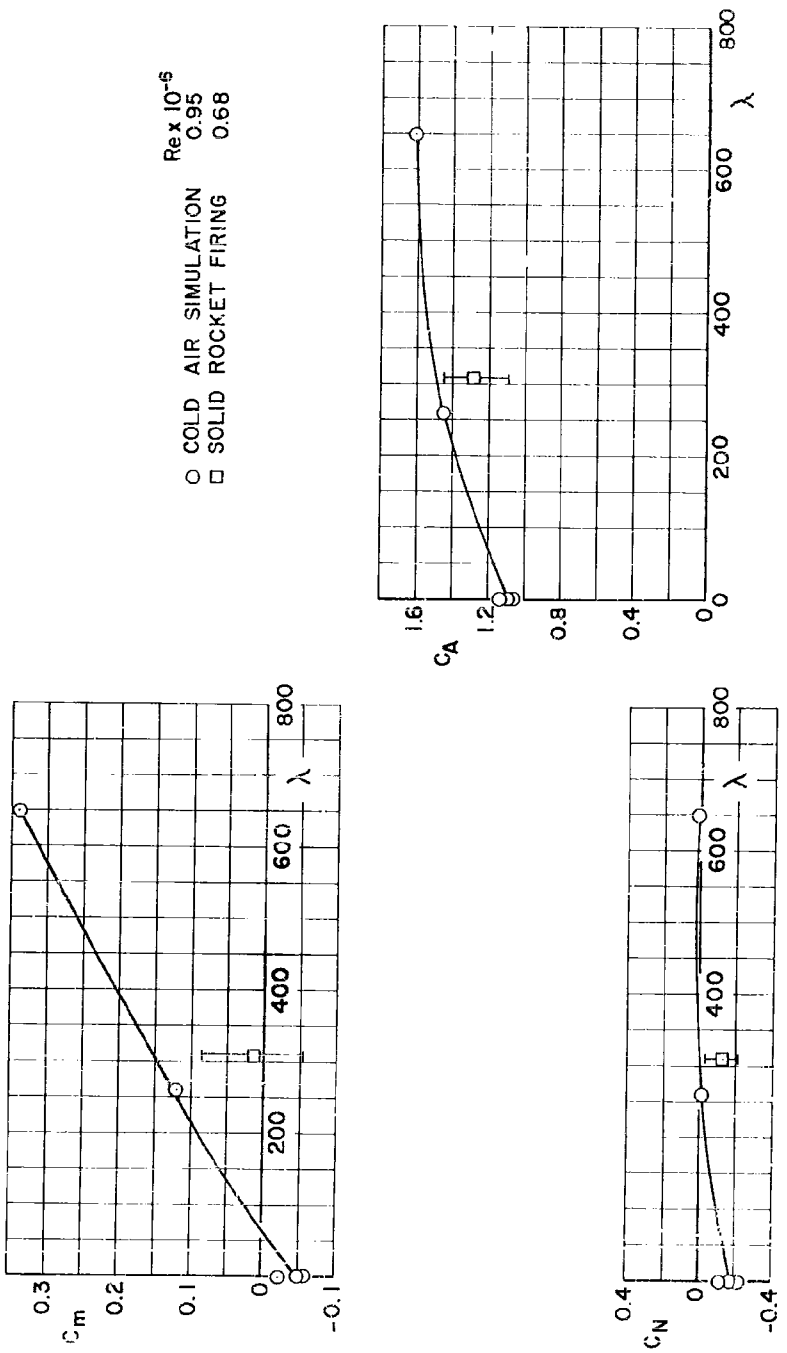

d. Crew Capsule with Parachute (BP_{31}) at Zero Angle of Attack

Fig. 19 Concluded

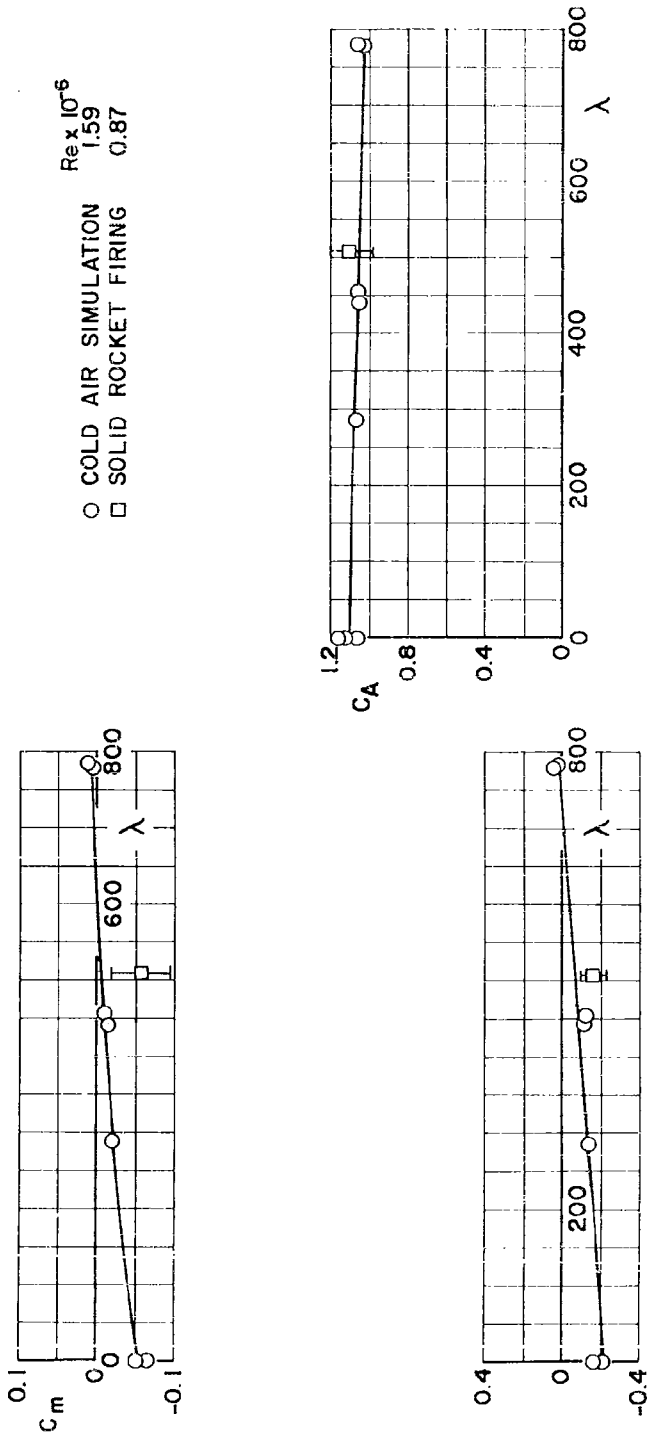

a. Crew Capsule (B) at Zero Angle of Attack

Fig. 20 Aerodynamic Coefficients for the Crew Capsule as a Function of Jet Pressure Ratio and Comparison with Rocket Firings at Mach Number 1.50

Cut on broken line

AEDC-TN-61-43

UNCLASSIFIED

Arnold Engineering Development Center, ARO, Inc., Arnold Air Force Station, Tennessee
STATIC STABILITY CHARACTERISTICS OF THE PROPOSED B-58 AIRCRAFT ESCAPE CAPSULE AT TRANSONIC MACH NUMBERS by L. E. Rittenhouse, D. J. Pierce, and W. E. Summers, May 1961. 72 pp. (ARO Project Nos. 221138 and 221089) (Program Area 102A) (AEDC-TN-61-43) (Contract No. AF 40(600)-800 S/A 11(60-110)). Unclassified

3 references

Results are presented from a wind tunnel investigation to ascertain the lateral and longitudinal stability and axial-force characteristics of the crew and pilot escape capsules proposed for the B-58 aircraft. The effect of varying several parachute parameters on parachute drag and capsule aerodynamics is also presented. Furthermore, a comparison of the capsule aerodynamic coefficients obtained with cold air simulation of the rocket exhausts in contrast to (over)

1. Airplanes--B-58
2. Airplanes--Safety measures
3. Escape capsules--Stability
4. Escape capsules--Transonic flow
5. Parachutes--Performance
I. Rittenhouse, L. E.
II. Pierce, D. J.
III. Summers, W. E.

UNCLASSIFIED

AEDC-TN-61-43

UNCLASSIFIED

Arnold Engineering Development Center, ARO, Inc., Arnold Air Force Station, Tennessee
STATIC STABILITY CHARACTERISTICS OF THE PROPOSED B-58 AIRCRAFT ESCAPE CAPSULE AT TRANSONIC MACH NUMBERS by L. E. Rittenhouse, D. J. Pierce, and W. E. Summers, May 1961. 72 pp. (ARO Project Nos. 221138 and 221089) (Program Area 102A) (AEDC-TN-61-43) (Contract No. AF 40(600)-800 S/A 11(60-110)). Unclassified

3 references

Results are presented from a wind tunnel investigation to ascertain the lateral and longitudinal stability and axial-force characteristics of the crew and pilot escape capsules proposed for the B-58 aircraft. The effect of varying several parachute parameters on parachute drag and capsule aerodynamics is also presented. Furthermore, a comparison of the capsule aerodynamic coefficients obtained with cold air simulation of the rocket exhausts in contrast to (over)

1. Airplanes--B-58
2. Airplanes--Safety measures
3. Escape capsules--Stability
4. Escape capsules--Transonic flow
5. Parachutes--Performance
I. Rittenhouse, L. E.
II. Pierce, D. J.
III. Summers, W. E.

UNCLASSIFIED

AEDC-TN-61-43

UNCLASSIFIED

Arnold Engineering Development Center, ARO, Inc., Arnold Air Force Station, Tennessee
STATIC STABILITY CHARACTERISTICS OF THE PROPOSED B-58 AIRCRAFT ESCAPE CAPSULE AT TRANSONIC MACH NUMBERS by L. E. Rittenhouse, D. J. Pierce, and W. E. Summers, May 1961. 72 pp. (ARO Project Nos. 221138 and 221089) (Program Area 102A) (AEDC-TN-61-43) (Contract No. AF 40(600)-800 S/A 11(60-110)). Unclassified

3 references

Results are presented from a wind tunnel investigation to ascertain the lateral and longitudinal stability and axial-force characteristics of the crew and pilot escape capsules proposed for the B-58 aircraft. The effect of varying several parachute parameters on parachute drag and capsule aerodynamics is also presented. Furthermore, a comparison of the capsule aerodynamic coefficients obtained with cold air simulation of the rocket exhausts in contrast to (over)

1. Airplanes--B-58
2. Airplanes--Safety measures
3. Escape capsules--Stability
4. Escape capsules--Transonic flow
5. Parachutes--Performance
I. Rittenhouse, L. E.
II. Pierce, D. J.
III. Summers, W. E.

UNCLASSIFIED

AEDC-TN-61-43

UNCLASSIFIED

Arnold Engineering Development Center, ARO, Inc., Arnold Air Force Station, Tennessee
STATIC STABILITY CHARACTERISTICS OF THE PROPOSED B-58 AIRCRAFT ESCAPE CAPSULE AT TRANSONIC MACH NUMBERS by L. E. Rittenhouse, D. J. Pierce, and W. E. Summers, May 1961. 72 pp. (ARO Project Nos. 221138 and 221089) (Program Area 102A) (AEDC-TN-61-43) (Contract No. AF 40(600)-800 S/A 11(60-110)). Unclassified

3 references

Results are presented from a wind tunnel investigation to ascertain the lateral and longitudinal stability and axial-force characteristics of the crew and pilot escape capsules proposed for the B-58 aircraft. The effect of varying several parachute parameters on parachute drag and capsule aerodynamics is also presented. Furthermore, a comparison of the capsule aerodynamic coefficients obtained with cold air simulation of the rocket exhausts in contrast to (over)

1. Airplanes--B-58
2. Airplanes--Safety measures
3. Escape capsules--Stability
4. Escape capsules--Transonic flow
5. Parachutes--Performance
I. Rittenhouse, L. E.
II. Pierce, D. J.
III. Summers, W. E.

UNCLASSIFIED

AEDC-TN-61-43

UNCLASSIFIED

rocket motor firings is discussed. The tests were conducted at Mach numbers 0.60, 0.93, and 1.50 at Reynolds numbers ranging from 0.40 to 2.20 million. The test article attitude was varied from -10 to 90 deg in the pitch plane and from -5 to 25 deg in the yaw plane. In general, both capsule configurations were statically unstable in the pitch and yaw planes. Furthermore, when the rocket jet was simulated, the parachute which was attached to the capsule dipped violently in and out of the jet wake.

UNCLASSIFIED

AEDC-TN-61-43

UNCLASSIFIED

rocket motor firings is discussed. The tests were conducted at Mach numbers 0.60, 0.93, and 1.50 at Reynolds numbers ranging from 0.40 to 2.20 million. The test article attitude was varied from -10 to 90 deg in the pitch plane and from -5 to 25 deg in the yaw plane. In general, both capsule configurations were statically unstable in the pitch and yaw planes. Furthermore, when the rocket jet was simulated, the parachute which was attached to the capsule dipped violently in and out of the jet wake.

UNCLASSIFIED

AEDC-TN-61-43

UNCLASSIFIED

rocket motor firings is discussed. The tests were conducted at Mach numbers 0.60, 0.93, and 1.50 at Reynolds numbers ranging from 0.40 to 2.20 million. The test article attitude was varied from -10 to 90 deg in the pitch plane and from -5 to 25 deg in the yaw plane. In general, both capsule configurations were statically unstable in the pitch and yaw planes. Furthermore, when the rocket jet was simulated, the parachute which was attached to the capsule dipped violently in and out of the jet wake.

UNCLASSIFIED

AEDC-TN-61-43

UNCLASSIFIED

rocket motor firings is discussed. The tests were conducted at Mach numbers 0.60, 0.93, and 1.50 at Reynolds numbers ranging from 0.40 to 2.20 million. The test article attitude was varied from -10 to 90 deg in the pitch plane and from -5 to 25 deg in the yaw plane. In general, both capsule configurations were statically unstable in the pitch and yaw planes. Furthermore, when the rocket jet was simulated, the parachute which was attached to the capsule dipped violently in and out of the jet wake.

UNCLASSIFIED